

**SURFACE ENHANCED INFRARED ABSORPTION SPECTROSCOPY:
A VALUABLE TECHNIQUE IN UNDERSTANDING GREEN CHEMISTRY**

by

Jeffrey Heyes

A thesis submitted to the Faculty of the University of Delaware in partial fulfillment of the requirements for the degree of Master of Chemical Engineering

Fall 2016

© 2016 Jeffrey Heyes
All Rights Reserved

ProQuest Number: 10246862

All rights reserved

INFORMATION TO ALL USERS

The quality of this reproduction is dependent upon the quality of the copy submitted.

In the unlikely event that the author did not send a complete manuscript and there are missing pages, these will be noted. Also, if material had to be removed, a note will indicate the deletion.



ProQuest 10246862

Published by ProQuest LLC (2017). Copyright of the Dissertation is held by the Author.

All rights reserved.

This work is protected against unauthorized copying under Title 17, United States Code
Microform Edition © ProQuest LLC.

ProQuest LLC.
789 East Eisenhower Parkway
P.O. Box 1346
Ann Arbor, MI 48106 – 1346

**SURFACE ENHANCED INFRARED ABSORPTION SPECTROSCOPY:
A VALUABLE TECHNIQUE IN UNDERSTANDING GREEN CHEMISTRY**

by

Jeffrey Heyes

Approved: _____
Bingjun Xu, Ph.D.
Professor in charge of thesis on behalf of the Advisory Committee

Approved: _____
Abraham M. Lenhoff, Ph.D.
Chair of the Department of Chemical and Biomolecular Engineering

Approved: _____
Babatunde A. Ogunnaike, Ph.D.
Dean of the College of Engineering

Approved: _____
Ann L. Ardis, Ph.D.
Senior Vice Provost for Graduate and Professional Education

ACKNOWLEDGMENTS

I would like to thank my family and friends for their emotional support through my thesis. I would also like to thank my advisor and lab mates for their intellectual contributions, advice, and support.

TABLE OF CONTENTS

| | |
|--|----|
| LIST OF FIGURES | vi |
| ABSTRACT | ix |
| Chapter | |
| 1 INTRODUCTION | 1 |
| 1.1 Electrochemistry for Carbon Neutrality | 1 |
| 1.2 Surface Enhanced Infrared Spectroscopy..... | 3 |
| 1.3 Thesis structure..... | 5 |
| 2 STUDIES OF CO ₂ REDUCTION ON PURE METAL SURFACES BY SURFACE ENHANCED INFRARED ADSORPTION SPECTROSCOPY | 6 |
| 2.1 CO ₂ Reduction on Cu at Low Overpotentials with Surface Enhanced In-Situ Spectroscopy | 6 |
| 2.1.1 Abstract..... | 6 |
| 2.1.2 Introduction | 7 |
| 2.1.3 Experimental..... | 9 |
| 2.1.3.1 In situ SEIRAS and electrochemical reactivity studies .. | 9 |
| 2.1.3.2 Characterization of the electrochemically deposited Cu film..... | 12 |
| 2.1.4 Results and Discussion | 14 |
| 2.1.4.1 Surface Sensitivity of the electrochemically deposited Cu film..... | 14 |
| 2.1.4.2 Identification of H _{ad} on Cu | 16 |
| 2.1.4.3 Coadsorption of H _{ad} and CO _{ad} on Cu | 18 |
| 2.1.4.4 Electrochemical reduction of CO ₂ on Cu at low overpotentials | 22 |
| 2.1.5 Conclusions | 23 |
| 2.2 CO ₂ reduction on Sn at Low Overpotentials with in-situ Surface Enhanced Spectroscopy..... | 24 |
| 2.2.1 Introduction | 24 |
| 2.2.2 Experimental..... | 25 |
| 2.2.3 Results and Analysis..... | 26 |
| 2.2.4 Conclusion..... | 29 |

| | | |
|----------|--|----|
| 3 | ELECTROCHEMICAL REDUCTION OF FURFURAL ON AU WITH IN-SITU SURFACE ENHANCED INFRARED ADSORPTION SPECTROSCOPY | 30 |
| 3.1 | Introduction | 30 |
| 3.2 | Experimental..... | 31 |
| 3.3 | Results and Discussion | 32 |
| 3.4 | Conclusion..... | 38 |
| 4 | CONCLUDING REMARKS AND FURTHER RESEARCH..... | 40 |
| | REFERENCES | 42 |
| Appendix | | |
| A | SUPPORTING INFORMATION | 49 |
| B | LEGAL PERMISSION | 60 |

LIST OF FIGURES

| | |
|--|----|
| Figure 1.1 Diagram of CO ₂ released into the atmosphere (values in Pg) (A) ^{2, 4} and how this inequality of the cycle is leading to increased atmospheric CO ₂ concentration (B) ³ | 1 |
| Figure 2.1 SEM image of (a) Au film electrolessly deposited on reflecting plane of Si wafer and (b) a Cu film electrochemically deposited atop the Au underlayer in our Cu deposition solution at 50mV for 180 s. | 13 |
| Figure 2.2 In-situ SEIRAS spectra of CO purged 0.5 M NaHCO ₃ using the Au underlayer (a) and the Cu film (b). Spectra were collected from bottom to top with a scan rate of 5 mV/s. | 14 |
| Figure 2.3 In-situ SEIRAS spectra on Cu in CO ₂ saturated 0.5 M NaHCO ₃ at (a) high and (b) low wavenumber region. Background spectrum taken at -0.1 V. Spectra were collected from bottom to top with a scan rate of 5 mV/s. The thick black trace represents the spectrum taken at -0.7 V. | 16 |
| Figure 2.4 (a) Time-resolved SEIRA spectra of H _{ad} Cu in CO ₂ saturated 0.5 M NaHCO ⁻³ at -0.5 V. (b) In-situ, time resolved adsorption of Ar purged solutions of 0.1 M NaClO ₄ in H ₂ O and D ₂ O and 0.2 M NaH ₂ PO ₂ in D ₂ O at -0.4 V on Cu, compared to a reference scan taken at -0.1 V. 4 cm ⁻¹ resolution, 64 co-added scans. | 18 |
| Figure 2.5 Time-resolved SEIRA spectra of co-adsorbed of CO _{ad} and H _{ad} (a) CO introduced to H _{ad} covered Cu surface. H _{ad} was accumulated on Cu at -0.5 V, and then the potential was increased to -0.4 V before CO was introduced. (c) H _{ad} accumulation on CO adsorbed Cu surface. CO was introduced to Cu at -0.05 V, then the potential was decreased to -0.4 V to accumulate H _{ad} on the Cu surface. Both sets of spectra were collected in 0.5 M NaHCO ₃ with the reference spectrum collected 0.05 V. (b) and (d) show integrated peak areas of CO _{ad} and H _{ad} bands after peak deconvolution, reported as a percentage of the largest H _{ad} peak, as a function of time for spectra presented in (a) and (b), respectively. Peak deconvolution spectra and procedures are provided in appendix A. | 21 |
| Figure 2.6 Faradaic efficiency for major products in CO ₂ saturated 0.5 M NaHCO ₃ on Cu foil from -0.2 V to -0.8 V. | 23 |
| Figure 2.7 SEM image of Sn film electrochemically deposited atop an Au underlayer on the reflective surface of a Si wafer in Sn plating solution for 7 min at -0.1 V. | 26 |

| | |
|---|----|
| Figure 2.8 In-situ SEIRAS spectra of CO ₂ purged 0.5 M NaHCO ₃ using Sn film, focusing on possible CO _{ad} band. Spectra were collected from bottom to top with a scan rate of 5 mV/s. Potential for each scan is given by the right axis. Background scan taken at -0.1 V. 4 cm ⁻¹ wavenumber resolution and 16 co-added scans. | 27 |
| Figure 2.9 In-situ SEIRAS spectra of CO ₂ purged 0.5 M NaHCO ₃ at given potential on right axis on Sn film. Reference scan taken at -0.1 V. 4 cm ⁻¹ resolution and 16 co-added scans. | 28 |
| Figure 3.1 NMR results comparing bands from Au foil reducing furfural at -1.0 V at the given charges passed with predicted 2-methylfuran band structure. ... | 32 |
| Figure 3.2 SEIRAS comparison of 2-methylfuran (red), furfuryl alcohol (blue), and furfural (black) at given concentrations at Au surface. All solutions are in a 0.1 M solution of HClO ₄ . No potential is applied and scans are at a 4 cm ⁻¹ wavenumber resolution. Background scan taken in pure 0.1 M HClO ₄ solution. | 34 |
| Figure 3.3 SEIRAS spectra of stepwise potential drop of 0.1 M HClO ₄ and 0.1 M furfural solution on Au film, purged in Ar. Scans are initially taken (purple) and taken again after 5 minutes (red). Reference scan taken in 0.1 M HClO ₄ at 0.6 V. Scans are taken at 4 cm ⁻¹ wavenumber resolution. | 36 |
| Figure 3.4 Time resolved SEIRAS spectra of furfural reduction on an Au film in a 0.1 M furfural and 0.1 M HClO ₄ solution. Purple and green traces represent potentials of -0.2 and -0.25 respectively. Reference spectrum is taken at 0.6 V in 0.1 M HClO ₄ . 64 co-added scans, 4 cm ⁻¹ resolution | 37 |
| Figure 3.5 Time resolved SEIRAS scans of 2-methylfuran remaining near the Au surface as the potential is raised from initial production at -0.3 V. Black scans indicate the initial scan taken at the given potential; red traces indicate spectra taken after the potential is maintained for 5 minutes. Reference scan taken at 0.6 V in 0.1 M HClO ₄ . 64 co-added scans; 4 cm ⁻¹ resolution. | 39 |
| Figure A.1 Schematic of the experimental setup used for SEIRAS experiments | 50 |
| Figure A.2 Schematic of the H-cell used for selectivity studies. Not pictured are two additional ports for headspace sampling and purging on the same side of the membrane as the working electrode. | 51 |

| | |
|--|----|
| Figure A.3 Cyclic voltammogram of 0.5 M NaHCO ₃ on electrochemically deposited Cu film saturated in Ar, CO ₂ and CO. The retardation of HER activity in the CO ₂ saturated electrolyte could be a CO ₂ reductive intermediate effect. CO similarly retards these reactions by site blocking for HER with a CO _{ad} species..... | 52 |
| Figure A.4 Peak deconvolution of Figure 2.1.5a(vii). Similar procedure was conducted for the rest of spectra in Figure 2.1.6a. Figure 2.1.6c are calculated based on the quantification of these deconvoluted peaks. Peak widths of the H _{ad} and CO _{ad} are fixed in the fitting, and similar procedure was employed in the fitting of Figure A.5..... | 53 |
| Figure A.5 Fitting of spectra in Figure 2.5b at times: 0 min (a), 5 min (b), 15 min (c), 25 min (d). Background fit is attributed to broad water character seen in Figure A.6. Note that the broad envelope from 2200-1975 cm ⁻¹ in Figure 2.6 is due to water rather than the H _{ad} or CO _{ad} band, which is confirmed by the spectrum of pure water. This broad band was removed in the peak deconvolution and quantification. | 54 |
| Figure A.6 Single reflectance ATR-FTIR spectra of H ₂ O on ZnSe prism, 4 cm ⁻¹ resolution. Peak centered at approx. 2350 cm ⁻¹ is ambient CO ₂ present in apparatus..... | 55 |
| Figure A.7 SEIRAS spectral comparison of CO _{ad} on Pt, Cu, and Au surfaces at indicated potentials. | 56 |
| Figure A.8 SEIRAS spectra (black traces) of 0.5 M NaHCO ₃ on Cu film with varying amounts of introduced formic acid at -0.4 V, with reference taken at -0.1 V in 0.5 M NaHCO ₃ prior to the introduction of formic acid. Concentrations are indicated by volume. ATR spectra of 0.1 M HCOONa and HCOOH on a Si crystal (red traces) are included for comparison. .. | 57 |
| Figure A.9 FTIR spectra of furfural and 2-methylfuran diluted with 0.1 M HClO ₄ on Si prism. 0.1 M HClO ₄ background, 64 co-added scans, 4 cm ⁻¹ wavenumber resolution. | 58 |
| Figure A.10 Time resolved SEIRAS spectra of 0.1 M furfural in 0.1 M HClO ₄ at open circuit potential. Reference taken at 0.6 V in 0.1 M HClO ₄ . 64 co-added scans, 4 cm ⁻¹ wavenumber resolution..... | 59 |

ABSTRACT

Green chemistry is presenting itself to be an important field in the future. In studying green electrochemical reactions, knowledge and understanding of surface adsorbed species can be vital in tuning these systems. *In-situ* surface enhanced spectroscopic investigations were conducted on several green systems. First, *in-situ* surface enhanced spectroscopic and reactivity investigations of the electrochemical reduction of CO₂ at low overpotentials (<0.7 V) were conducted on Cu surfaces. Vibrational bands corresponding to adsorbed hydrogen (H_{ad}) and carbon monoxide (CO_{ad}) on Cu have been identified at 2090 cm⁻¹ and 2060 cm⁻¹, respectively. Spectroscopic investigations show that H_{ad} is capable of partially displacing CO_{ad}; however, CO_{ad} is unable to displace H_{ad} to any detectable level. The preferential adsorption of H over CO on Cu is consistent with the high selectivity towards the hydrogen evolution reaction at potentials > -0.8 V vs. RHE. CO₂ reduction was also investigated on Sn under similar conditions. CO_{ad} is tentatively identified at low potentials (-0.2 to -0.7 V) at approximately 1925 cm⁻¹. Local bulk concentrations of formate were also identified at higher potentials (0.3 V). Similarly, *in-situ* spectroscopic techniques were used to identify and follow surface concentrations of methylfuran in the reduction of furfural on Au. At low overpotentials (-0.2 V), local concentrations of 2-methylfuran are produced persist to potentials of 1.2 V. This high local concentration may lead to low performance of furfural reduction on Au. Combined, these studies show the capabilities of surface enhanced spectroscopic studies.

Chapter 1

INTRODUCTION

1.1 Electrochemistry for Carbon Neutrality

Non-renewable fossil fuels constitute the vast majority of energy sources used for both transportation and energy production¹. This utilization of carbon-based fuels causes an imbalance in the natural carbon cycle that occurs naturally across the world². Prior to these fuels being used, this carbon cycle was largely maintained, changing only with major events on the Earth surface². Since fossil fuels have been used, this cycle has been disrupted, with a great deal more CO₂ being produced in energy, industrial, and transportation systems than is used naturally² (Figure 1.1A). This has led to an

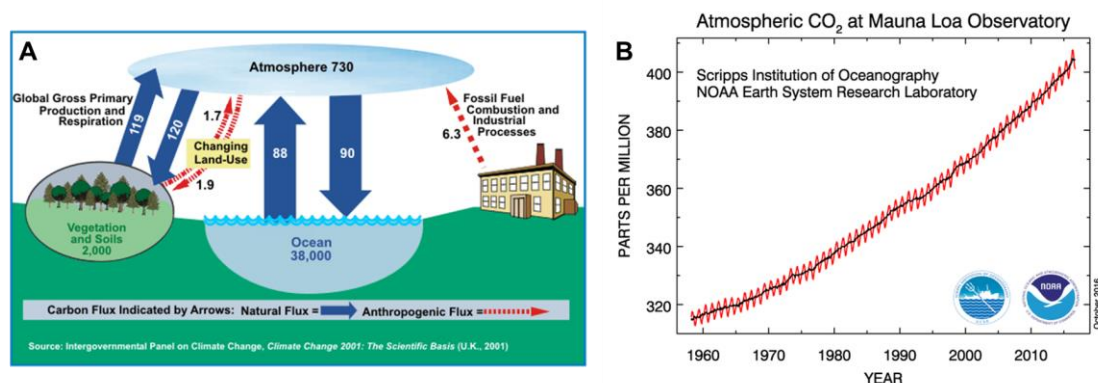


Figure 1.1 Diagram of CO₂ released into the atmosphere (values in Pg) (A)^{2, 4} and how this inequality of the cycle is leading to increased atmospheric CO₂ concentration (B)³.

abundance of CO₂, which can easily be seen while following atmospheric CO₂ concentrations over the past 50 or so years (Figure 1.1B).³

With the consistent increase atmospheric CO₂ (Figure 1.1A), actions need to be taken to remove this gaseous product. The most evident route would be to diminish the amount of CO₂ that is released into the atmosphere, but predictions show that major negative effects of global climate change would still occur if even drastic measures are taken against emissions alone⁵. In order to reduce the amount of CO₂ in the atmosphere, direct sequestration measures must be taken. Systems have been implemented to collect CO₂ from power plants⁶, and atmospheric CO₂ can be sequestered into deep underground reservoirs that had previously stored fossil fuels⁷. By utilizing sequestered CO₂ for value added products, individuals and corporations would be incentivized collect and use CO₂.

One method of CO₂ utilization is electrochemical reduction. In general, this method takes dissolved CO₂ in equilibrium with bicarbonate in solution at mild temperatures and pressures, and applies a negative current working electrode where the CO₂ is reduced to value added products⁸⁻⁹. Years of research have produced a vast collection of electrodes and electrolytes that have shown promise in CO₂ reduction, but currently fall short in efficiency and selectivity⁸.

A dissimilar idea for closing the carbon cycle comes from utilization of biomass upgrading¹⁰. Biomass derivatives represent a large collection of materials derived from plant mass. The ideal situation is upgrading of lignocellulosic biomass, which constitutes non-edible plant mass¹¹. These derivatives can be subcategorized into three

distinct categories. The first category is lignin, which is comprised of methoxylated phenylpropane monomers to form a largely unusable, amorphous polymer. This small portion (10%) can be separated from the biomass, leaving the more valuable fractions intact. Hemicellulose is the second biomass fraction. Slightly more abundant than lignin (25-35%), hemicellulose is again an amorphous polymer but the monomers that comprise hemicellulose are primarily sugars. The sugars contained in hemicellulose are the easiest to extract of the 3 fractions, and yields are in the range of 90%. Cellulose is the final biomass fraction. Unlike its amorphous counterparts, cellulose is polymer comprised of linked glucose monomers. Using cellulose, biological conversion gives the highest glucose yields, while hydrolysis promotes the production of decompositions to 5-hydroxymethylfuran, levulinic acid, and low value humins¹⁰. Upgrading of these three lignocellulose derivatives offers a much lower cost path for creating fuels and fuel additives, and does not cut into available food supplies. Further, lignocellulose materials can be more efficiently produced if efficient upgrading is possible, and the cycle of growth of biomass and burning of biofuels would be carbon neutral¹².

1.2 Surface Enhanced Infrared Spectroscopy

While looking at reduction mechanisms, understanding metal electrode/electrolyte interaction is vital to developing mechanisms and engineering solutions to improve production, and surface sensitive spectroscopic techniques can be employed to study these systems. Subtractively normalized interfacial FTIR (SNIFTIRS)¹³⁻¹⁷ and reflection-adsorption spectroscopy (RAS)¹⁸ use a low IR

interfering window, generally made of CaF_2 , to propagate an incident IR beam through the electrolyte, reflecting off the electrode surface, and traveling back through the electrolyte and the window material to be collected and detected. While techniques such as SNIFTIRS¹⁵ and RAS have been previously used to study these spectro/electrochemical systems¹³⁻¹⁷, interference from the relatively thick (several μm)¹⁸ electrolyte layer causes difficulties in observing adsorbed species on the electrode surface¹⁹. Transportation complications are also indicated while utilizing a small electrolyte volume for the reactions studied as the reactant cannot be effectively transported to the electrode surface, and the electrode surface is slow to react to external potential changes in the systems¹⁹⁻²¹. These reflectance set-ups do allow for enhanced surface sensitivity, but to alleviate complications therein, surface enhanced IR adsorption spectroscopy(SEIRAS) is used.

SEIRAS is based on an ATR configuration instead of using a P-polarized IR beam reflected from the metal electrode surface as seen in the SNIFTIR technique^{15, 22}. In a standard ATR configuration, an incident IR beam penetrates the ATR active prism (Si, CaF_2 , ZnSe), totally reflecting internally at the far surface. This produces an evanescent wave that propagates on the order of 1-2 μm beyond the reflecting plane. SEIRAS combines this with a surface plasmon radiation enhancement²¹. By using this enhancement, thin metal films deposited electrolessly, physically, or electrochemically can interact with IR radiation to produce localized plasmon modes. These plasmon modes are generated via the polarization of the small islands in the metal films by incident IR photons¹⁹, and this polarization induces a dipole which enhances the local

EM field²³⁻²⁵. Chemisorption of the metal film improves this enhancement more than physisorbed films²¹. Chemisorption thus plays a role in the enhancing effect, but reasons for this are currently not well understood. SEIRAS utilizes this enhanced local field to improve sensitivity of species 5-10 nm from the thin island film's surface by a factor of 10-1000²¹. This allows for sensitivity towards adsorbed species without severe transport limitation, intense electrolyte interference, or delayed surface response to external potential variation, and generates signal from adsorbates at intensities similar to that from the electrolyte. With improved sensitivity towards adsorbed surface species, we can then investigate adsorbate/electrode and electrolyte/electrode interfaces *in-situ* and derive a better understanding of reactions and reaction mechanisms.

1.3 Thesis structure

With respect to this work, two different chemical systems are observed. In the second chapter, adsorption of CO and its further reduction to value-added products as CO₂ reduction are observed on Cu electrodes. Similar work is conducted for CO₂ reduction on Sn. In the third chapter, the second system observes surface chemistry in the reduction of furfural into 2-methylfuran on an Au electrode. Both systems use this enhancing effect to better understand the chemistry occurring at the surface/electrolyte interface via this surface enhancing technique.

Chapter 2

STUDIES OF CO₂ REDUCTION ON PURE METAL SURFACES BY SURFACE ENHANCED INFRARED ADSORPTION SPECTROSCOPY

2.1 CO₂ Reduction on Cu at Low Overpotentials with Surface Enhanced In-Situ Spectroscopy

This work has been adapted with permission from Heyes, J.; Dunwell, M.; Xu, B. CO₂ Reduction on Cu at Low Overpotentials with Surface-Enhanced in Situ Spectroscopy. *The Journal of Physical Chemistry C* **2016**, 120 (31), 17334-17341.). Copyright 2016 American Chemical Society

2.1.1 Abstract

In-situ surface enhanced spectroscopic and reactivity investigations of the electrochemical reduction of CO₂ at low overpotentials (<0.7 V) was conducted on Cu surfaces. Vibrational bands corresponding to adsorbed hydrogen (H_{ad}) and carbon monoxide (CO_{ad}) on Cu have been identified at 2090 cm⁻¹ and 2060 cm⁻¹, respectively. Spectroscopic investigations show that H_{ad} is capable of partially displacing CO_{ad}; however, CO_{ad} is unable to displace H_{ad} to any detectable level. The preferential adsorption of H over CO on Cu is consistent with the high selectivity towards the hydrogen evolution reaction at potentials > -0.8 V vs. RHE.

2.1.2 Introduction

Climate change, caused largely by the anthropogenic CO₂ emissions, has been a rising concern over the past several decades²⁶⁻²⁹. With the atmospheric CO₂ concentration surpassing 400 ppm³⁰, efficient and affordable processes need to be put in place to capture and utilize atmospheric CO₂, as emission-cutting programs alone are unlikely to be sufficient to reduce the atmospheric CO₂ to the preindustrial level³¹. Combining renewable energy sources with efficient electrochemical processes could provide a viable pathway to not only reduce the amount of atmospheric CO₂, but also utilize CO₂ as a platform in the generation of fuels and chemicals⁸. Of the monometallic catalysts tested, only copper has shown appreciable selectivity to short-chain hydrocarbons and oxygenates³²⁻³⁶. Overpotentials higher than 1 V are needed to produce these desired products of CO₂ reduction on Cu, and selectivity control remains challenging³⁵. Understanding how reactions proceed on the molecular level at the electrolyte/electrode interface could provide guiding principles for future catalyst design.

Much research effort has been dedicated to the development of efficient and selective processes for electrochemical reduction of CO₂ on Cu electrodes^{8, 32-53}. These studies demonstrate the production of methane, ethylene, ethanol, and formate^{32-35, 37-41, 44-45, 50-52}, however, direct evidence of surface adsorbed reaction intermediates, and in turn mechanistic understanding, has been lacking. Of the various mechanisms proposed, the most agreed upon intermediate is CO^{33, 35, 37-39, 44, 46-49, 52} which has been used to generate similar products to those from CO₂ reduction^{44, 46, 52, 54}. Computational studies

have shown that the adsorption energy of CO on Cu is ideal for further reduction, in contrast to Pt and Ag, which CO binds too strongly⁵⁵ and too weakly^{47, 55}, respectively. From CO, many further surface intermediates have been proposed^{35, 37-39 53}, albeit without direct experimental evidence. In this regard, spectroscopic studies will be informative in elucidating the reaction mechanism. However, spectroscopic studies^{13-14, 17, 56-67} of the surface-mediated electrochemical reduction of CO₂ are challenging, primarily due to the difficulty in differentiating the signal originating from the electrode/electrolyte interface from that of the bulk electrolyte and reactants, whose spectral features typically overwhelm those of reaction intermediates. Several spectroscopic techniques have been employed in the investigations of CO₂ electrochemical reduction, including attenuated total reflection (ATR)-FTIR spectroscopy⁶⁴, sum-frequency generation (SFG)⁶⁶, and surface enhanced Raman spectroscopy (SERS).⁶⁷ In particular, SNIFTIRS (subtractively normalized interfacial FTIR spectroscopy)¹⁵, which achieves surface sensitivity by taking advantage of differences spectra obtained using p and s polarized light, has been used to identify adsorbed reaction intermediates, e.g., CO_{ad}, on several metal surfaces, i.e., Cu^{13, 16-17}, Ni¹⁴, and Ag¹³. Reflection-based FTIR techniques, e.g., SNIFTIRS, typically employ a thin layer electrolyte configuration¹⁵, where the working electrode is pushed flush against the IR window creating a thin layer of electrolyte (several microns in thickness) around the electrode. This thin layer configuration could cause mass transport limitations,²¹ especially at high reaction rates and for gas evolving reactions such as HER and CO production from CO₂ reduction.

Herein, we report an *in-situ*, surface-sensitive spectroscopic study of electrochemical reduction of CO₂ on Cu in the low overpotential range (0.1 – 0.7 V). The employment of surface-enhanced infrared absorption spectroscopy (SEIRAS) with an ATR configuration allows for the identification of adsorbed surface intermediates while sampling directly into the bulk of the electrolyte, without the severe transport problems encountered using SNIFTIRS. The surface sensitivity of this technique (~10 nm from the electrode surface) originates from the attenuation of the infrared beam due to the high angle of incidence and the selective amplification of the resultant evanescent wave near the electrode by plasmon resonance within the thin film electrode.¹⁹⁻²¹ Many metals, including Cu, have been demonstrated to be SEIRAS active⁶⁸⁻⁶⁹. SEIRAS was employed in a previous study on CO₂ reduction on Pt⁷⁰ in H₂SO₄ as a side reaction in the hydrogen fuel cell. In the present study, we have identified adsorbed atomic hydrogen (H_{ad}) on Cu in the potential range of -0.15 to -0.65 V by a combination of ATR-SEIRAS and isotopic labeling techniques. H_{ad} appears able to partially displace adsorbed CO (CO_{ad}); however, the reverse displacement does not occur. Correlations between the spectroscopic and reactivity studies are discussed.

2.1.3 Experimental

2.1.3.1 In situ SEIRAS and electrochemical reactivity studies

The Au film underlayer is prepared following a variation of reported electroless Au deposition techniques⁷¹⁻⁷². Si ATR prisms are polished with a 0.05 μm Al₂O₃

suspension and cleaned in alternating baths of acetone and double DI water with sonication. The prisms then are immersed in a bath of room temperature piranha etch (3:1 volumetric ratio of 95-98% H_2SO_4 (Sigma-Aldrich) and 30% H_2O_2 (Sigma-Aldrich)) for 20 min to remove organic surface impurities. After a thorough water rinse to remove all piranha etch, the reflecting plane of the prism is submerged in 40% NH_4F (Sigma-Aldrich) for 70-90 s to form a hydrogen terminated Si surface⁷³, which is then immersed in the mixture of the Au plating solution (5.75 mM $\text{NaAuCl}_4 \cdot 2\text{H}_2\text{O}$ + 0.025 M NH_4Cl + 0.075 M Na_2SO_3 + 0.025 M $\text{Na}_2\text{S}_2\text{O}_3 \cdot 5\text{H}_2\text{O}$ + 0.026 M NaOH) and a 2 wt% hydrofluoric acid solution (in a 9:2 ratio) at 55 °C for 4 min.

Cu is electrochemically deposited on the Au underlayer. The deposition cell consists of three electrodes, with the Au underlayer as the working electrode, an Ag/AgCl reference electrode and a graphite rod counter electrode. The Cu plating solution is used as the electrolyte (0.1 M H_2SO_4 (99% Sigma-Aldrich) and 5.75 mM CuSO_4 (99.998% Sigma-Aldrich)). A potential of 0.05 V vs. RHE (all voltages in this work are referenced to the reversible hydrogen electrode, RHE, unless noted otherwise) was applied for 3 min to achieve the desired film thickness of ~15 nm, estimated based on total charge passed. Cu films are used immediately upon deposition.

0.5 M NaHCO_3 solution is prepared by bubbling 0.25 M Na_2CO_3 (99.998%, Sigma Aldrich in water) with CO_2 (99.99%, Keen Gas) for at least 4 h to ensure the electrolyte is saturated with CO_2 , then purified with iminodiacetate resin (Cheelex®-100, Bio-Rad Laboratories, Inc.) for at least 1 hour to remove trace metal impurities³⁵. 0.1 M NaClO_4 solution is prepared by dissolving solid NaClO_4 (99.99%, Sigma-

Aldrich) in double distilled water or D₂O (>99.8%, Acros Organics). Additional samples are saturated with CO (99.9% Keen Gas) or Ar (99.99% Keen Gas).

The Cu-coated Si ATR crystal is placed in a two-compartment, three-electrode spectroelectrochemical cell (Figure A.1). The counter electrode (a graphite rod) is separated from the working and reference electrodes, i.e., the Cu film and a saturated Ag/AgCl electrode, respectively, with a piece of anion exchange membrane (FAA, Fumatech). The only stirring effect within the cell is from various gasses bubbled. This cell is integrated into the Agilent Technologies Cary 660 FTIR spectrometer with a modified Pike Technology VeeMax II accessory at a 60° incident angle. Electrochemical measurements are carried out with a SOLARTRON 1260/1287 system. All spectroscopic experiments are conducted at a 4 cm⁻¹ spectral resolution. Spectra are presented in absorbance, with positive and negative peaks showing an increase and decrease in signal, respectively.

Electrochemical reactivity studies are performed on Cu foil (99.998% Sigma-Aldrich) in an air-tight, two-compartment, three electrode glass electrochemical cell (Figure A.2). The Cu working electrode and the reference electrode (Ag/AgCl) are placed in the same, stirred compartment (125 RPM), while the counter electrode (a graphite rod) is separated by a piece of anion exchange membrane (FAA, Fumatech). Prior to electrolysis, the Cu foil is cleaned by a ~10 s immersion in aqua regia (3:1 volumetric ratio of 70% HCl (Fischer Scientific) and 70% HNO₃ (Sigma Aldrich)) and thoroughly rinsed with water. Gas phase products are sampled manually with an airtight syringe and analyzed with an Agilent Technologies 7890B gas chromatograph (GC).

The GC is equipped with an ShinCarbon ST 100/120 column (Restek), a methanizer, a flame ionization detector (FID), and a thermal conductance detector (TCD) for the separation and quantification of products. Ar is used as the carrier gas to enhance the sensitivity of H₂ in the TCD. Quantification of dissolved formate is conducted by ¹H-NMR (JEOL AVIII600) via calibration from integrated peak area ratios with a DMSO/D₂O internal standard and known concentrations of formate. A Princeton Applied Research VersaSTAT3 is used for electrochemical measurements.

Scanning electron microscopic images of the electrochemical deposited Cu films (JEOL JSM 7400F) show a similar rough morphology to that of the underlying Au film with an acceleration voltage of 3.0 kV. The composition of deposited metal films is monitored by the energy dispersive X-ray spectroscopic (EDX) system with an ultra-thin window Si-Li X-ray detector.

2.1.3.2 Characterization of the electrochemically deposited Cu film

The electrochemically deposited Cu film has a very similar rough morphology to that of the underlying Au film (Figure 2.1a). Cu films used in this study are prepared by electrochemically depositing Cu on an Au underlayer, which is chemically deposited on a Si ATR crystal. EDX confirms that only Cu, Au and Si are present. The roughness of the metal film is vital to its surface sensitivity in the spectroscopic study¹⁹⁻²¹, and SEM images of both the Au underlayer and the Cu film show a rough morphology (Figure 2.1b), with the island size of the Cu film (50-75 nm) slightly larger than that of

the Au film. The thickness of the Cu film is estimated to be ~15 nm based on the charge passed in the electrochemical deposition. The Cu film used in the SEIRAS studies show similar voltammograms to those on bulk polycrystalline Cu (Figure A.3) in absence and presence of CO₂.

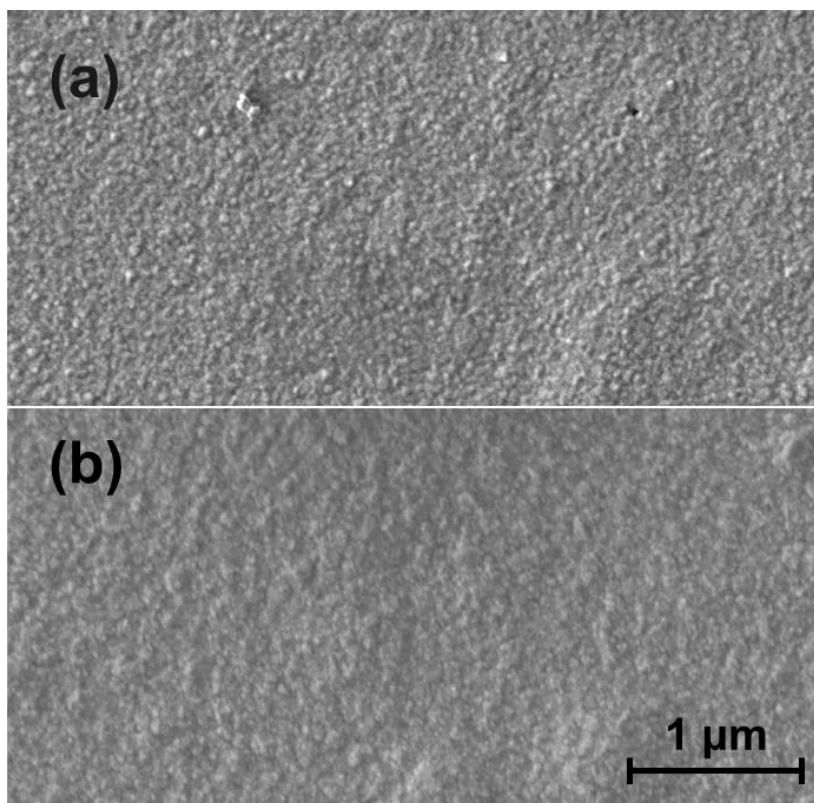


Figure 2.1 SEM image of (a) Au film electrolessly deposited on reflecting plane of Si wafer and (b) a Cu film electrochemically deposited atop the Au underlayer in our Cu deposition solution at 50mV for 180 s.

2.1.4 Results and Discussion

2.1.4.1 Surface Sensitivity of the electrochemically deposited Cu film

The observation of characteristic spectral features of adsorbed H, CO, and carbonate shows the Cu film is SEIRAS active without exposed Au. To verify that the electrochemically deposited Cu film completely covers the underlying Au surface, CO

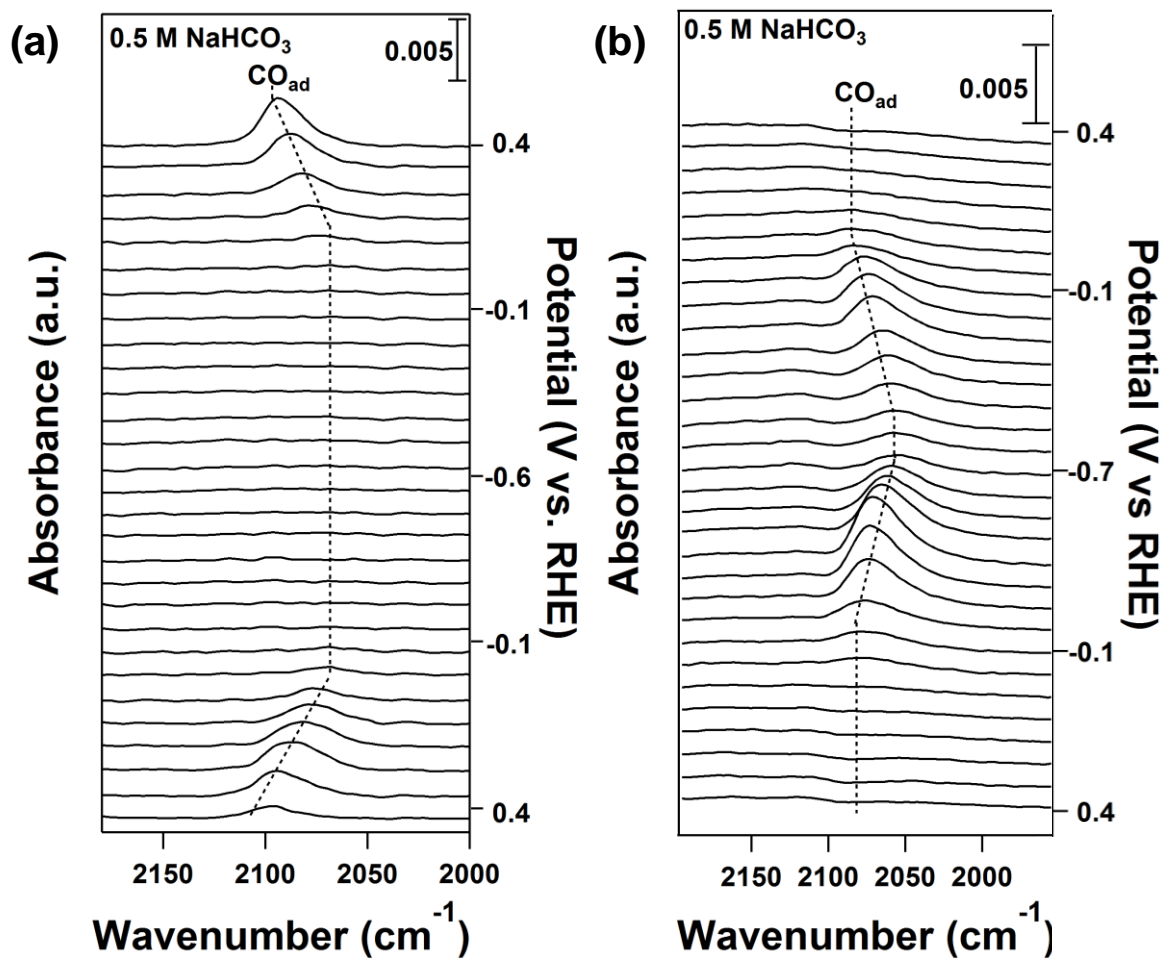


Figure 2.2 In-situ SEIRAS spectra of CO purged 0.5 M NaHCO₃ using the Au underlayer (a) and the Cu film (b). Spectra were collected from bottom to top with a scan rate of 5 mV/s.

was introduced as a probe molecule⁷⁴. The vibrational bands for adsorbed CO appear at different wavenumbers and potential ranges on Au (Figure 2.2a) and Cu (Figure 2.2b). The band corresponding to linearly adsorbed CO on Au appears at 2136 cm⁻¹ at 0.4 V vs. RHE (all potentials in this work are referenced to the reversible hydrogen electrode (RHE), unless noted otherwise), and gradually redshifts and weakens to 2110 cm⁻¹ as the potential decreases to 0 V, which is consistent with the literature⁷⁵. The disappearance of adsorbed CO at low potential on Au could be caused by displacement of CO_{ad} by electrostatically adsorbed cations⁷⁶⁻⁷⁷ or reaction intermediates in HER. The shift of peak position with the electrode potential is due to the Stark tuning effect, which is indicative of adsorbed species⁷⁸. In contrast, a 2070 cm⁻¹ band corresponding to linearly bond CO_{ad}⁶⁸ on Cu appears at -0.1 V (Figure 2.2b), which redshifts to 2058 cm⁻¹ as the potential decreases to -0.7 V. This is close to the CO_{ad} bands observed previously at similar potentials on Cu with SNIFTIRS^{17, 33} and SEIRAS⁶⁸. The absence of the band corresponding to CO adsorbed on Au sites on the film indicates that the Au underlayer is completely covered by electrochemically deposited Cu. A strong vibrational band at 1510 cm⁻¹ appears at 0.4 V, which reduces in intensity and redshifts to 1429 cm⁻¹ as the electrode potential decreases to -0.3 V. The peak position and intensity shift reversibly with potential in cyclic potential scans (only once cycle presented in Figure 2.3), which is attributed to adsorbed CO₃²⁻ (CO₃²⁻_{ad}) on the Cu surface (Figure 2.1.3b). Similar potential dependent behavior of adsorbed carbonate has been reported on Au, however,

the band corresponding to adsorbed carbonate appears on Au at potentials above 0.4 V.⁷⁹

2.1.4.2 Identification of H_{ad} on Cu

Adsorbed hydrogen, which could be an important reaction intermediate in the electrochemical reduction of CO_2 and HER, is identified on the Cu surface using SEIRAS. A weak but distinct band at 2090 cm^{-1} was observed in the potential range of -0.15 to -0.65 V on Cu in CO_2 -saturated 0.5 M $NaHCO_3$ during the potential cycle

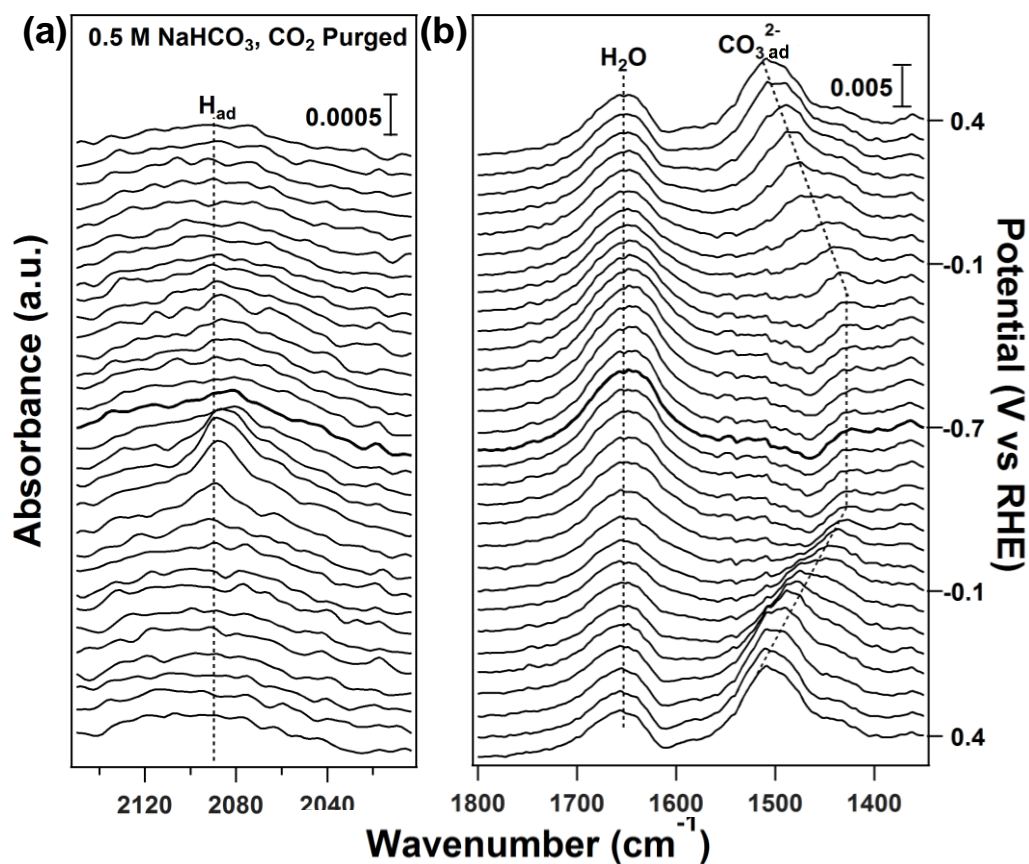


Figure 2.3 In-situ SEIRAS spectra on Cu in CO_2 saturated 0.5 M $NaHCO_3$ at (a) high and (b) low wavenumber region. Background spectrum taken at -0.1 V. Spectra were collected from bottom to top with a scan rate of 5 mV/s. The thick black trace represents the spectrum taken at -0.7 V.

(Figure 2.3a). Moreover, the intensity of this band grew over the course of 30 min at -0.5 V (Figure 2.4a). This band is unlikely to be CO_{ad} , because the peak position of CO_{ad} on Cu at the same potential was observed at 2070 cm^{-1} (Figure 2.2b), 20 cm^{-1} lower than the observed peak. Moreover, a similar band appears at 2090 cm^{-1} when the experiment was carried out on Cu in Ar-purged 0.1 M NaClO_4 (Figure 2.4b), in which no carbon-containing compound exists, excluding the possibility of CO production. Furthermore, the 2090 cm^{-1} band disappeared when a similar experiment was conducted in 0.1 M NaClO_4 in D_2O , and a band at 1480 cm^{-1} was observed, which is consistent with the expected isotopic shift from H_{ad} to D_{ad} (Figure 2.4b). This offers further support for the H_{ad} assignment. Another possible identification for this peak is a Cu-carbonyl species, which has been previously reported to appear at 2107 cm^{-1} in a phosphate solution,⁵⁷ but observation of the 2090 cm^{-1} peak without CO_2 , the isotopic shift and the lack of phosphate in the electrolyte indicate this alternative identification is unlikely. Additionally, the amount of a Cu-carbonyl species should increase with increasing electrode potential, which is opposite of the observed behavior of the 2090 cm^{-1} peak. All results are consistent with the assignment that the band centered at 2090 cm^{-1} corresponds to H_{ad} . The absence of the H_{ad} band in previous reflection absorption FTIR spectroscopic studies^{13, 17, 68} could be due to the lack of sufficient surface sensitivity and/or sufficient time for H_{ad} to accumulate. Calculations of the H_{ad} band have been shown to be lower in wavenumber (1013 and 862 cm^{-1})⁸⁰ for 3-fold sites, but due to the IR absorption of the Si ATR crystal in this region, we cannot detect these bands⁸¹. The

lack of the H_{ad} band in the anodic scan in Figure 2.3a could be due to the high surface coverage of electrostatically bound cations at low potentials^{76, 82-84}.

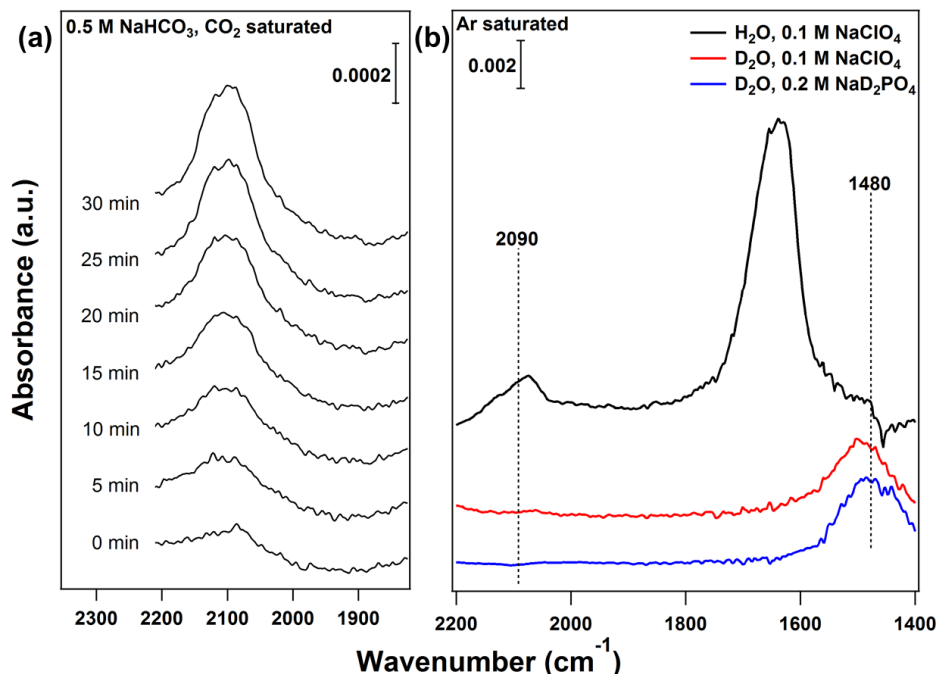


Figure 2.4 (a) Time-resolved SEIRA spectra of H_{ad} Cu in CO_2 saturated 0.5 M $NaHCO_3$ at -0.5 V. (b) In-situ, time resolved adsorption of Ar purged solutions of 0.1 M $NaClO_4$ in H_2O and D_2O and 0.2 M NaH_2PO_2 in D_2O at -0.4 V on Cu, compared to a reference scan taken at -0.1 V. 4 cm^{-1} resolution, 64 co-added scans.

2.1.4.3 Coadsorption of H_{ad} and CO_{ad} on Cu

Both CO_{ad} and H_{ad} are potential surface reaction intermediates in the electrochemical reduction of CO_2 ^{35, 37-39, 41, 53} whereas H_{ad} is the key intermediate for HER. Thus, the coadsorption or competitive adsorption of CO_{ad} and H_{ad} on the catalyst surface could have significant impact on product distribution. H_{ad} was first accumulated at -0.5 V, at which potential the H_{ad} band is most intense (Figure 2.3a), on Cu for 30 min before the potential was increased to -0.4 V (Figure 2.5a(i)). At this potential, both the CO_{ad} and

H_{ad} bands are sufficiently large in magnitude and distinct in wavenumber for further analysis and peak deconvolution (Figure 2.2b and 2.3a). CO was then introduced to the H_{ad} covered Cu surface by purging the system with gaseous CO. The CO_{ad} band (2070 cm^{-1}) grew over the course of 30 min (Figure 2.5a(i-vii)). Peak deconvolution (Figures A.4 and A.5) shows that the integrated area of the H_{ad} band increases by 40% as the intensity of the CO_{ad} band grows within 30 min, indicating that CO_{ad} does not displace H_{ad} at the studied potential (Figure 2.5b). No clear sign of CO_{ad} was observed when maintaining the Cu electrode at -0.4 or -0.5 V in Ar saturated 0.5 M $NaHCO_3$. Reversing the sequence in which H_{ad} and CO_{ad} were introduced shows that H_{ad} is able to partially displace CO_{ad} . CO was introduced to the Cu surface at -0.05 V (where there is no significant growth of the H_{ad} peak) in a 0.5 M $NaHCO_3$ electrolyte until the CO_{ad} band stopped growing to produce a CO_{ad} covered Cu surface without accumulating any H_{ad} (Figure 2.5c(i)). The potential of the CO_{ad} covered Cu surface was then lowered to -0.4 V. The ability of H_{ad} to displace CO_{ad} indicates that the higher bonding energy species (H_{ad})⁸⁵ displaces the species with lower bonding energy (CO_{ad})⁴⁸ at the same linearly bonded adsorption site³⁹. The integrated area of the CO_{ad} band decreases by ~50% (Figure 2.5d) by the time that the H_{ad} band has ceased changing with time (Figure 2.5c(v)). Also, the position of CO_{ad} shifts from 2057 cm^{-1} in the absence of coadsorbed H_{ad} to 2067 cm^{-1} with coadsorbed H_{ad} , which is likely caused by the decrease in coverage. The difference between the final spectra in Figures 2.5a and 2.5b is due in part to water feature that appears in this spectral region (Figure A.6), which is accounted for in the spectral deconvolution. A true equilibrium state was not reached during the

course of the experiment as the final spectra of displacement experiments (~30 min) are still different. The gradual drift in the water background over a long period of time, e.g., over 1 h, makes the comparison of spectra unreliable. It is important to note that the absolute integrated peak areas cannot be directly used to compare absolute coverages of multiple species (due to differences in extinction coefficients for different adsorbates), but can be used to obtain time resolved accumulation or diminishment for a single adsorbed species.

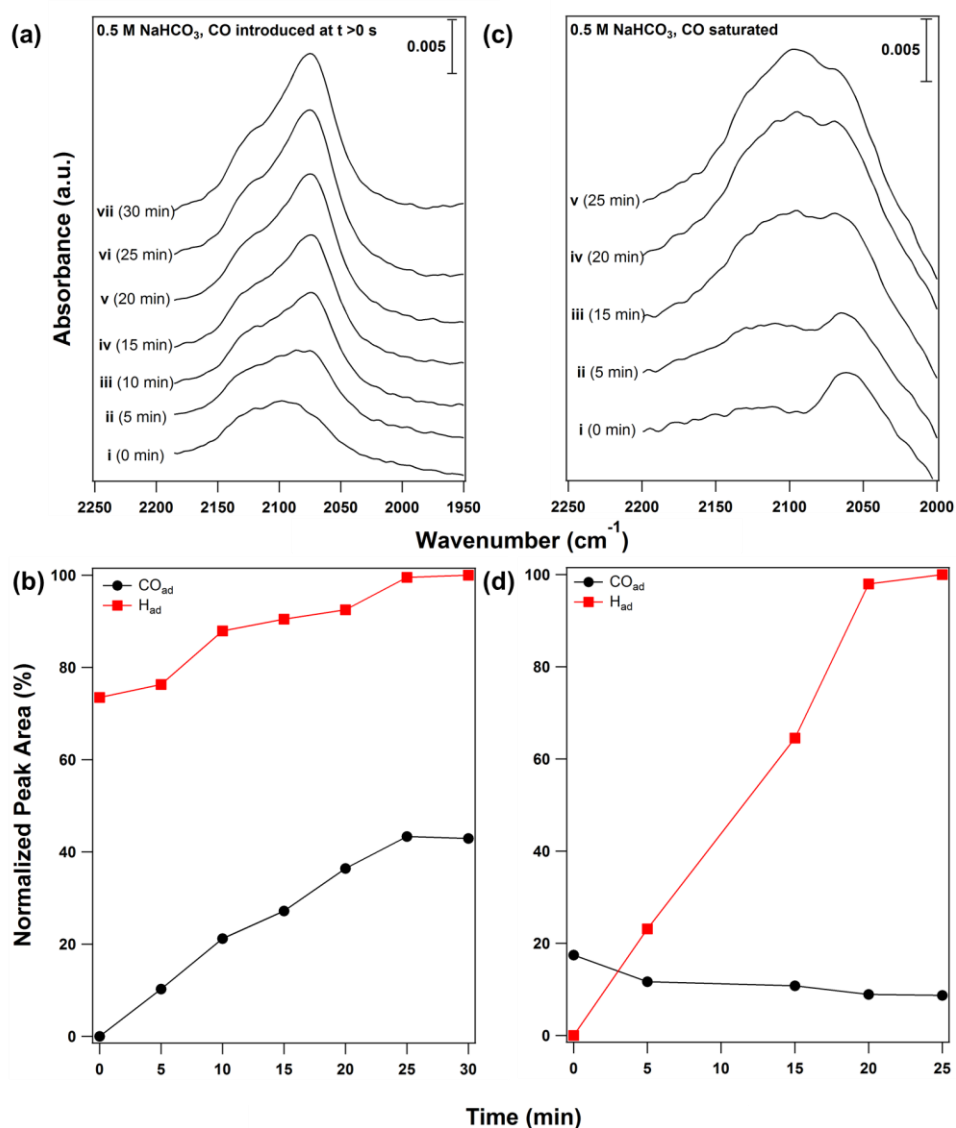


Figure 2.5 Time-resolved SEIRA spectra of co-adsorbed of CO_{ad} and H_{ad} (a) CO introduced to H_{ad} covered Cu surface. H_{ad} was accumulated on Cu at -0.5 V, and then the potential was increased to -0.4 V before CO was introduced. (c) H_{ad} accumulation on CO adsorbed Cu surface. CO was introduced to Cu at -0.05 V, then the potential was decreased to -0.4 V to accumulate H_{ad} on the Cu surface. Both sets of spectra were collected in 0.5 M NaHCO_3 with the reference spectrum collected 0.05 V. (b) and (d) show integrated peak areas of CO_{ad} and H_{ad} bands after peak deconvolution, reported as a percentage of the largest H_{ad} peak, as a function of time for spectra presented in (a) and (b), respectively. Peak deconvolution spectra and procedures are provided in appendix A.

2.1.4.4 Electrochemical reduction of CO₂ on Cu at low overpotentials

High faradaic efficiency towards HER observed in experiments on a Cu foil is consistent with the observed evolution of the H_{ad} band and its ability to displace CO_{ad} on Cu surface in the potential range of -0.2 to -0.8 V. Product distribution of electrochemical reduction of CO₂ on a Cu foil in a three electrode H-cell with CO₂-saturated 0.5 M NaHCO₃ has been determined in the potential range of -0.2 to -0.8 V (Figure 2.6). Close to 90% charge balance is obtained for experiments over the whole potential range tested, indicating no significant product is missing. About 60% of charge is used in the production of formate at -0.2 V. The low selectivity of HER can be attributed to low H_{ad} coverage at this potential. The lack of a detectable spectral feature from formate with SEIRAS is due to limited coverage and the low concentration of formate formed in the bulk. SEIRAS does not show any formate features until the concentration reactions 5000 PPM (Figure A.8), well above the approximately 20 PPM concentrations found in reactivity studies. HER dominates at potentials from -0.4 to -0.8 V, with a Faradaic efficiency of close to 80% and persists high at potentials where H_{ad} is no longer observed (-0.8 V), which is consistent with previous work.³⁵ The absence of H_{ad} at potential lower than -0.7 V could be attributed to two causes: (1) increased rate for the associative desorption of H_{ad} that reduces H_{ad} coverage, and (2) displacement of H_{ad} by non-covalently bonded cations (Na⁺)^{76, 82-84}. The diminishment of the CO_{ad} band at potential below -0.5 V can also be explained by the stronger adsorption of sodium cations in solution. Only a minor fraction of charge (<5%) contributes to the production of formate and CO in this potential range. This is

consistent with the stronger adsorption of H_{ad} than CO_{ad} , which promote selectivity toward CO over formate. No spectroscopic signature of reaction intermediates leading to formate production are detected; this is most likely due to the transient nature of these species and low surface coverage. Low residence time combined with low surface coverage make such species difficult to detect using SEIRAS.

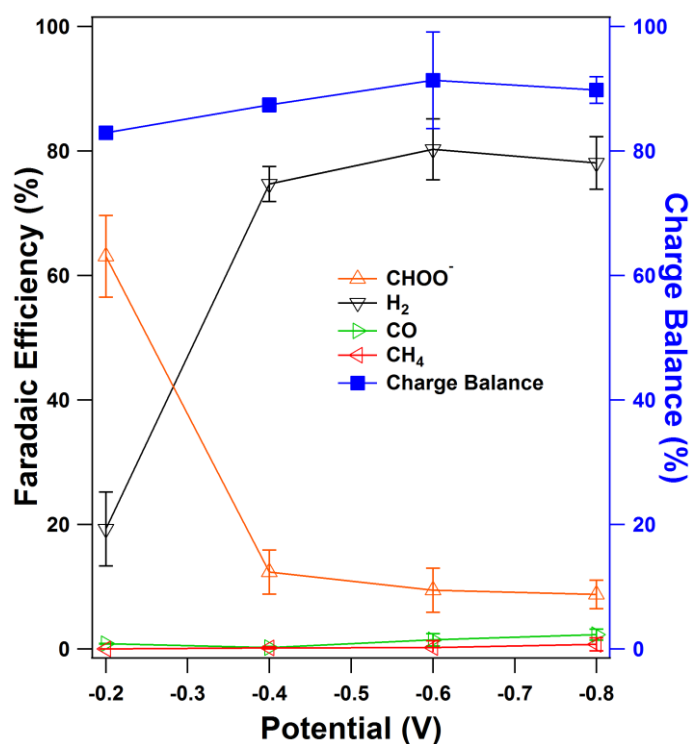


Figure 2.6 Faradaic efficiency for major products in CO_2 saturated 0.5 M $NaHCO_3$ on Cu foil from -0.2 V to -0.8 V.

2.1.5 Conclusions

In summary, SEIRAS studies of the electrochemical reduction of CO_2 on the Cu surface in the potential range of -0.2 to -0.8 V identified H_{ad} and CO_{ad} , both of which

are key reaction intermediates in the electroreduction of CO₂. H_{ad} is able to partially displace CO_{ad}, while the reverse displacement does not occur, which indicates H_{ad} adsorbed more strongly on Cu than CO_{ad} in the potential range studied. The high selectivity for HER and low selectivity for CO production are consistent with the spectroscopic results. Furthermore, the diminishment and disappearance of bands corresponding to H_{ad} and CO_{ad} at low potentials (< -0.5 V) indicate the surface coverage and residence time of those intermediates are likely to be low at potentials typically employed for hydrocarbon and oxygenate production from electrochemical reduction of CO₂.

2.2 CO₂ reduction on Sn at Low Overpotentials with in-situ Surface Enhanced Spectroscopy

2.2.1 Introduction

From the initial work on Cu, a similar initial study was conducted with Sn. While not as varied in products⁹, Sn can provide valuable insight into the class of primarily formate producing species⁹. Although unlikely as a catalyst itself, Sn is exceptionally cost effective, and is one of the least costly materials shown to be functional in CO₂ reduction at 1% the cost of Cu⁸⁶. Compared to many of the products seen from Cu that can be directly used as fuel, formate is a lower value product, but still a great deal more valuable than CO₂.

Direct studies of Sn are limited; it is normally considered as one of many catalysts^{9, 34, 40, 63}. Spectroscopic tests of Sn are limited, but tin has been shown to

interact through a thin surface oxide phase on the electrode surface⁶⁴. Using a similar technique to our copper investigation, initial studies of CO₂ reduction on Tin are conducted, but nothing of note is detected.

2.2.2 Experimental

The majority of the techniques described in section 2.1.3.1 remain unchanged here. However, instead of an electrochemical deposition of Cu as that section described, the Au underlayer is instead immersed in a solution of 0.01 M SnCl₂ (99.99%, Sigma Aldrich) and 0.8 M Citric Acid, triammonium (97%, Arcos Organics), based on previous electrochemical deposition techniques of Sn⁸⁷. A potential of -0.1 V is applied to the surface for 7 min for an approximate 10-20 nm of deposited Sn. The difference in the film surface from copper can be seen in Figure 2.7, using the same microscope and conditions as section 2.1.3.1. Small pinholes (50-100 nm across) appear in the surface, but the majority of the surface >95% keep Sn characteristics. Similar to the Cu surface (Figure 2.1), the retains the surface roughness of the underlaying Au film. These films are then placed in the same apparatus, use the same instruments, and utilize the same electrolyte as described in section 2.1.3.1.

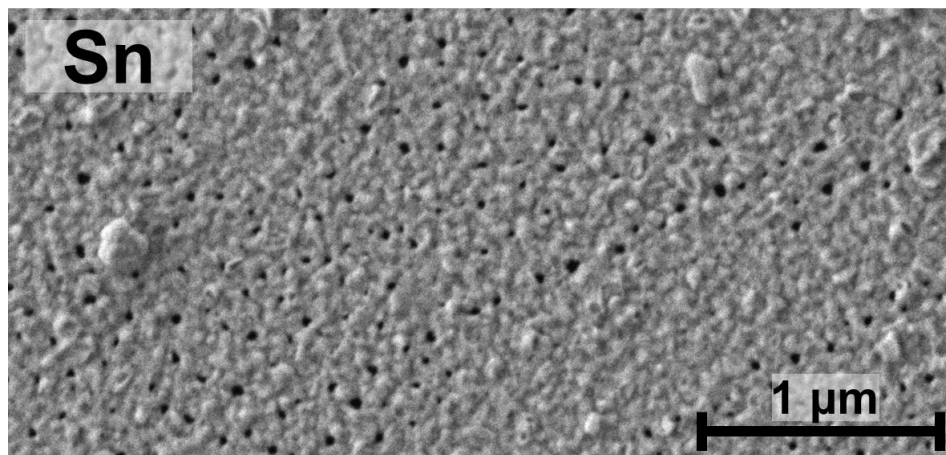


Figure 2.7 SEM image of Sn film electrochemically deposited atop an Au underlayer on the reflective surface of a Si wafer in Sn plating solution for 7 min at -0.1 V.

2.2.3 Results and Analysis

Limited species are detected on the Sn surface. Adsorption in the wavenumber region common to CO adsorption is observed⁸⁸ (Figure 2.8). This could be adsorption on the Sn surface, or, potentially, CO adsorption on the Au underlayer; the CO reaching this surface via pinholes. Comparing the potential at which this band is observed to that of CO adsorption in Figure 2.2, this is unlikely as Au adsorbs CO at wavenumbers more than 100 cm^{-1} higher than seen on Sn and at a much higher potential (0.3 V). Observing CO_{ad} on the Sn surface is unexpected because amount of CO produced should be about 1/10 that of formate⁹. Further testing would be necessary to confirm this band as CO. However, indications of Stark Tuning effects give evidence that the Sn film made is indeed surface sensitive⁷⁸.

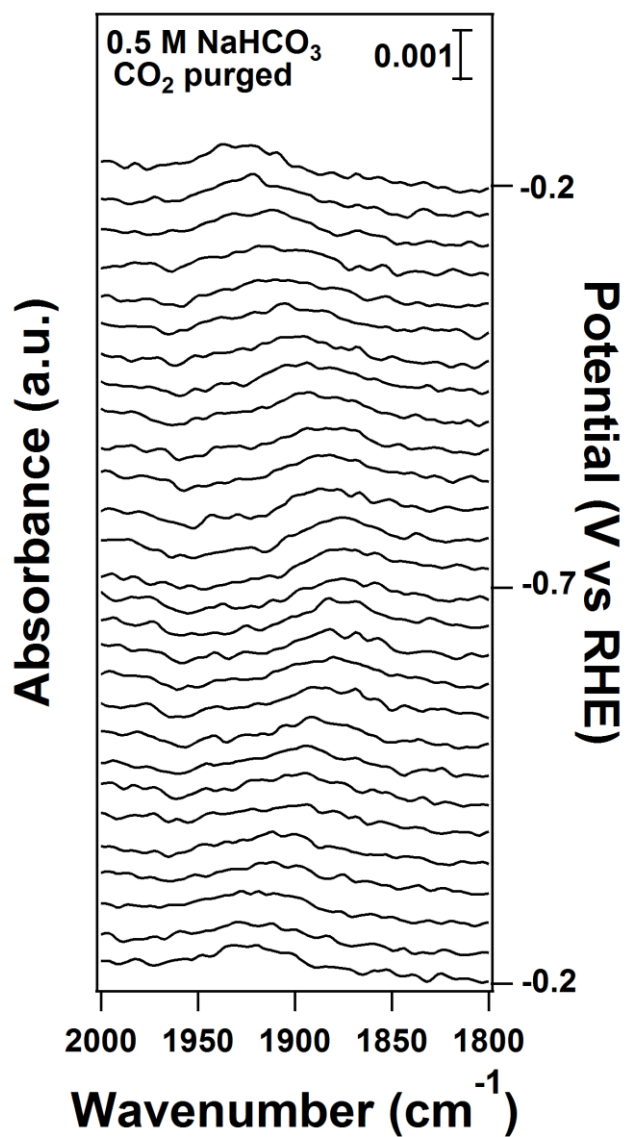


Figure 2.8 In-situ SEIRAS spectra of CO₂ purged 0.5 M NaHCO₃ using Sn film, focusing on possible CO_{ad} band. Spectra were collected from bottom to top with a scan rate of 5 mV/s. Potential for each scan is given by the right axis. Background scan taken at -0.1 V. 4 cm⁻¹ wavenumber resolution and 16 co-added scans.

Aside from CO, it is important to detect the major product, formate⁹, while using a technique such as SEIRAS. Formate is produced, as is evidenced when the film undergoes a potential cycle (Figure 2.9). When at higher potentials (near 0.3 V), a small broad band appears at about 1570 cm⁻¹, but at lower potentials, this band diminishes. The wavenumber of this band is comparable to that seen in bulk sodium formate on Si and Cu (1580 cm⁻¹) (Figure A.8). As the band only appears to change in intensity and not peak location, it is likely that the negatively charged formate species is merely attracted to the Sn surface at high potentials, but does not adsorb on the Sn surface.

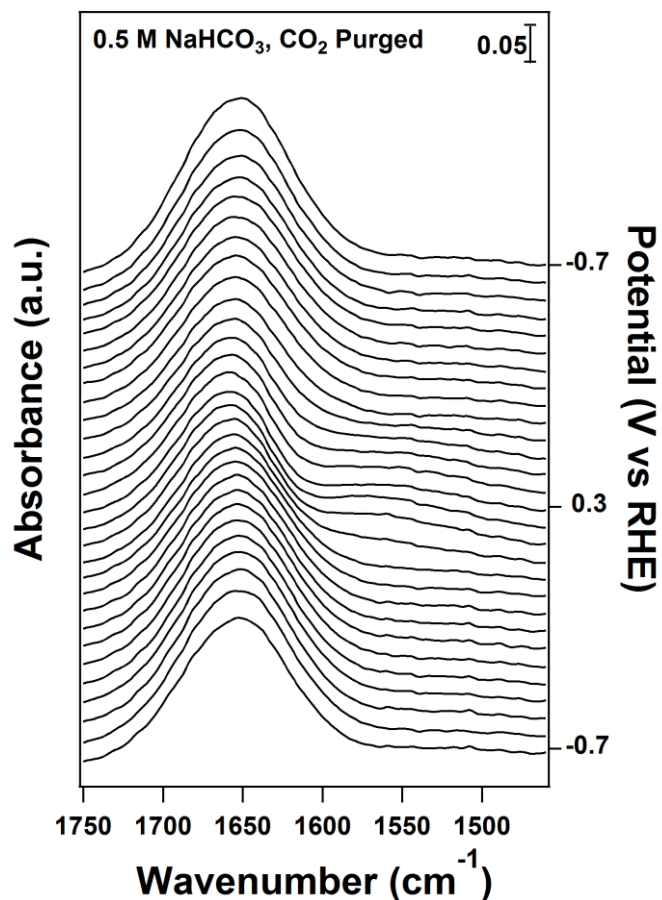


Figure 2.9 In-situ SEIRAS spectra of CO₂ purged 0.5 M NaHCO₃ at given potential on right axis on Sn film. Reference scan taken at -0.1 V. 4 cm⁻¹ resolution and 16 co-added scans.

2.2.4 Conclusion

While producing a surface sensitive Sn film utilizing a similar technique to deposition of Cu films on Au is worthwhile, the Sn does not show any new data about surface reactions occurring during the reduction of CO₂ on Sn. Some aspects of this preliminary work could be continued, such as further identifying CO_{ad} on the Sn surface and optimizing the Sn plating solution and technique, but the initial results do not show any new or promising avenues for further study. Sn presents itself as one of primarily formate producing species, and gaining understanding into this separate class of CO₂ reduction electrodes is valuable. However, it appears as if SEIRAS is unable to provide any additional details to this specific reduction reaction.

Chapter 3

ELECTROCHEMICAL REDUCTION OF FURFURAL ON AU WITH IN-SITU SURFACE ENHANCED INFRARED ADSORPTION SPECTROSCOPY

3.1 Introduction

Processes have been described using full sugar molecules directly for fuel production. Another pathway for important platform chemicals and fuels is through furanics⁸⁹⁻⁹⁰. Both furfural and HMF are important intermediates for these value added products, and are produced from xylose from hemicellulose and glucose from cellulose, respectively, at relatively high yields. For the purposes of this study, focus will be placed on the reduction of furfural to 2-methylfuran. Furfural reduces through furfuryl alcohol, which can be used as a solvent and resin, to 2-methylfuran, which can be used directly as fuel, or can be converted via ring opening to diesel or jet fuels⁹⁰. The possibility of reduction of furfural to 2-methylfuran has been known for many years⁹¹ with several studies being conducted⁹², but previous studies have primarily focused on its reduction with Pt⁹¹⁻⁹⁵ and Cu^{91, 93, 96}.

Using furfural as a model compound for biomass derived feedstock, surface enhanced IR spectroscopy (SEIRAS) is used to investigate the reaction *in-situ*. While previous reports have looked at a variety of biomass molecules, electrodes, and electrolyte systems with involved with furfural reduction⁹¹⁻⁹⁶, no work has been conducted spectroscopically, and surface sensitive work has only been tentatively related to biomass reduction and computational⁹⁷. Using SEIRAS, insight into the surface of the Au film can be garnered, and used to better understand and optimize this

reduction. A batch set-up spectro-electrochemical cell is used to examine this reaction *in-situ*.

3.2 Experimental

Prior to spectroscopic investigations, initial reduction of furfural on an Au foil was conducted using the standard electrochemical cell depicted in appendix A-2. Prior to the experiment, both chambers are thoroughly rinsed with double deionized water before being assembled into the two compartment configuration. A graphite rod counter electrode in 10 ml of 0.1 M HClO₄ (70%, Sigma Aldrich) acts as the counter electrode, with a Nafion 1135 membrane separating it from the working electrode. The working electrolyte is 0.1 M HClO₄ combined with 0.1 M furfural (99%, Sigma Aldrich) unless otherwise noted, and the reference electrode is a saturated Ag/AgCl electrode. A gold foil (99.99%, Alfa-Aesar) is used for initial selectivity testing and is prepared by a 30 s soak in freshly prepared piranha etch (1:3 Hydrogen peroxide (25%, Sigma Aldrich) : sulfuric acid (70% Fischer Scientific) to remove any remaining surface organics. For the spectroscopic experiments, a Solartron 1260/1287 potentiostat system is used to carry out electrochemical measurements. A JEOL AVIII600 NMR is used to monitor concentrations in resulting solutions.

Spectroscopic results utilize the Au underlayer film as the working electrode, details of which are found in section 2.1.3.1. The setup is similar to that found in Figure A.1, and the counter electrode and membrane remain the same from the selectivity study in the previous paragraph. A saturated Ag/AgCl reference electrode is placed close to

the Au films surface. This cell is then loaded into a VeeMax 2 platform, and loaded into an Agilent Technologies Cary 660 FTIR spectrometer.

3.3 Results and Discussion

Prior to spectral analysis, Au needed to be tested as a catalyst for furfural reduction. While Au had been used in similar reduction chemistries in the past⁹⁸, gold's use in this reaction has not been previously shown. Using a gold foil, 0.1 M furfural in 0.1 M HClO₄ is reduced at -1.0 V for 1 kC, and samples are taken every 250 C.

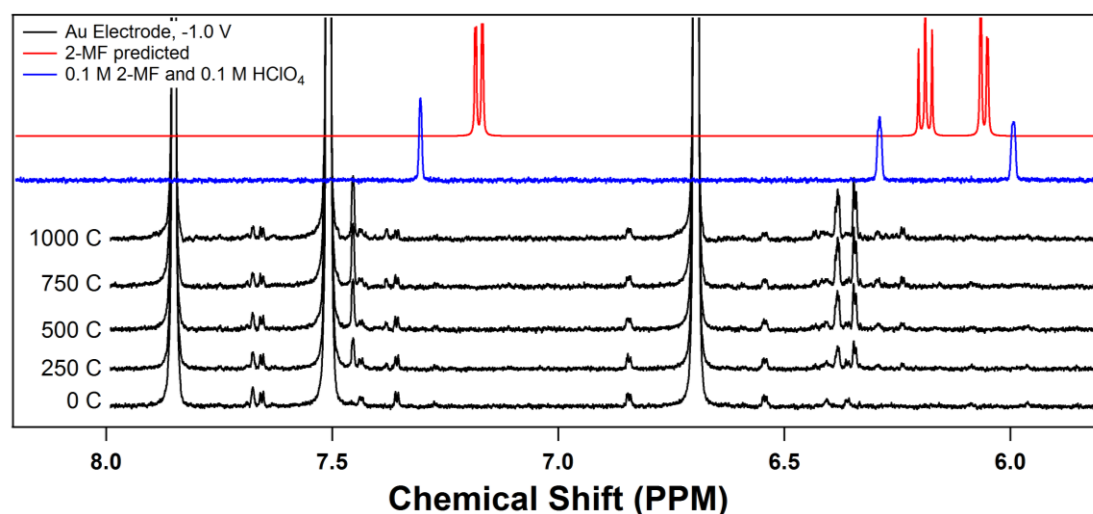


Figure 3.1 NMR results comparing bands from Au foil reducing furfural at -1.0 V at the given charges passed with predicted 2-methylfuran band structure.

Figure 3.1 shows NMR results each sample taken and scaled samples of furfuryl alcohol and 2-methylfuran, likely reduction products⁹⁵. Over this period of charge, bands arise that coincide with bands of 2-methylfuran. However, there are no indications of furfuryl alcohol in these samples. Previous studies have shown stronger indications that furfuryl

alcohol is an intermediate in the reduction, but the results here do not necessarily agree with this conclusion⁹⁵.

Once Au was shown to produce 2-methylfuran, bands related to this reaction must be identified as SEIRAS can produce bands not seen simply on Si (Figure A.9). By introducing external sources for the expected species present, one can identify how the individual species interacts not only in the perchlorate environment, but also how it interacts with the Au surface. In Figure 3.2, the three main species of interest, furfural, 2-methylfuran, and fufuryl alcohol, are all introduced to an Au film at varying concentrations mixed with 0.1 M HClO₄. While a number of bands arise compared to the HClO₄ background scan, the major indicating band for 2-methylfuran here is 1512 cm⁻¹, and furfural has independent character at 1666 cm⁻¹. Furfuryl alcohol shows a unique band at 1420 cm⁻¹. Many of the other bands seen in these materials shares a wavenumber region that makes it difficult to independently identify a given species due to overlap. For purposes in IR identifications, these peaks are used. Band identification and relative strength can give an order of magnitude estimation of concentrations of these species near the Au surface; differences in Au films make a direct comparison to concentrations unreliable.

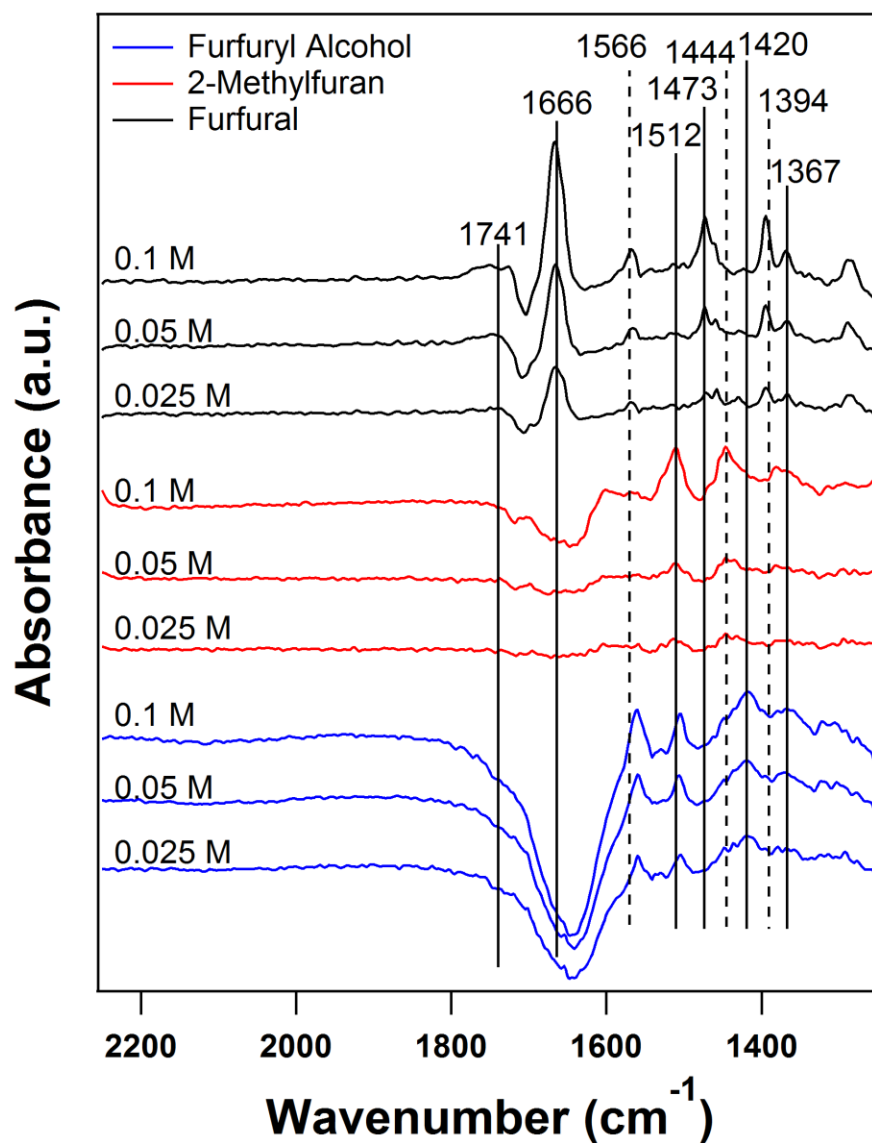


Figure 3.2 SEIRAS comparison of 2-methylfuran (red), furfuryl alcohol (blue), and furfural (black) at given concentrations at Au surface. All solutions are in a 0.1 M solution of HClO_4 . No potential is applied and scans are at a 4 cm^{-1} wavenumber resolution. Background scan taken in pure 0.1 M HClO_4 solution.

Once the bands that indicate specific species are identified, the potential at which furfural is first reduced is found (Figure 3.3). As the potential is stepwisely lowered in an Ar purged 0.1 M HClO₄ and 0.1 M furfural electrolyte on Au, a band begins to appear at 1508 cm⁻¹. This band, which can be identified as bulk 2-methylfuran (Figures 3.2 and A.9), starts to appear after several minutes at -0.1 V. This band increases when the potential is decreased to -0.2 V and grows further at -0.3 V. 2-Methylfuran is thus produced at relatively high potentials on Au compared to the -1.0 V standard reduction potential⁹⁵. Comparing to the control, the concentration near the Au surface is relatively high compared to the concentrations seen in the bulk, which are below the detection limit of ¹H NMR. This difference in concentration could be attributed to the low solubility of 2-methylfuran in aqueous solutions such that the methylfuran produced stays local to the Au surface. It has also been postulated that during the production of 2-methylfuran the product undergoes resinification⁹³, which could prevent activity on the Au surface and increase local 2-methylfuran concentration. Growth of this band with time is also important to demonstrate that this change is not simply due to an imposed current on the Au surface. Here, there is a time resolved set of spectra, and the spectrum show a temporal dependence of 2-methylfuran production as time passes at -0.2 V (Figure 3.4). As the Au film electrode is maintained at this potential for a 30-minute period, the near surface concentration of 2-methylfuran increases. When the potential is further reduced to -0.25 V, the band indicative of 2-methylfuran, 1508 cm⁻¹, increases at a greater rate. This is not an effect of time on the Au surface; furfural on Au without an imposed potential is maintained in this timeframe (Figure A.10). The band is thus

showing the production of 2-methylfuran and is not an effect of adsorption of a species with a like band or a reaction that occurs independently in the electrolyte.

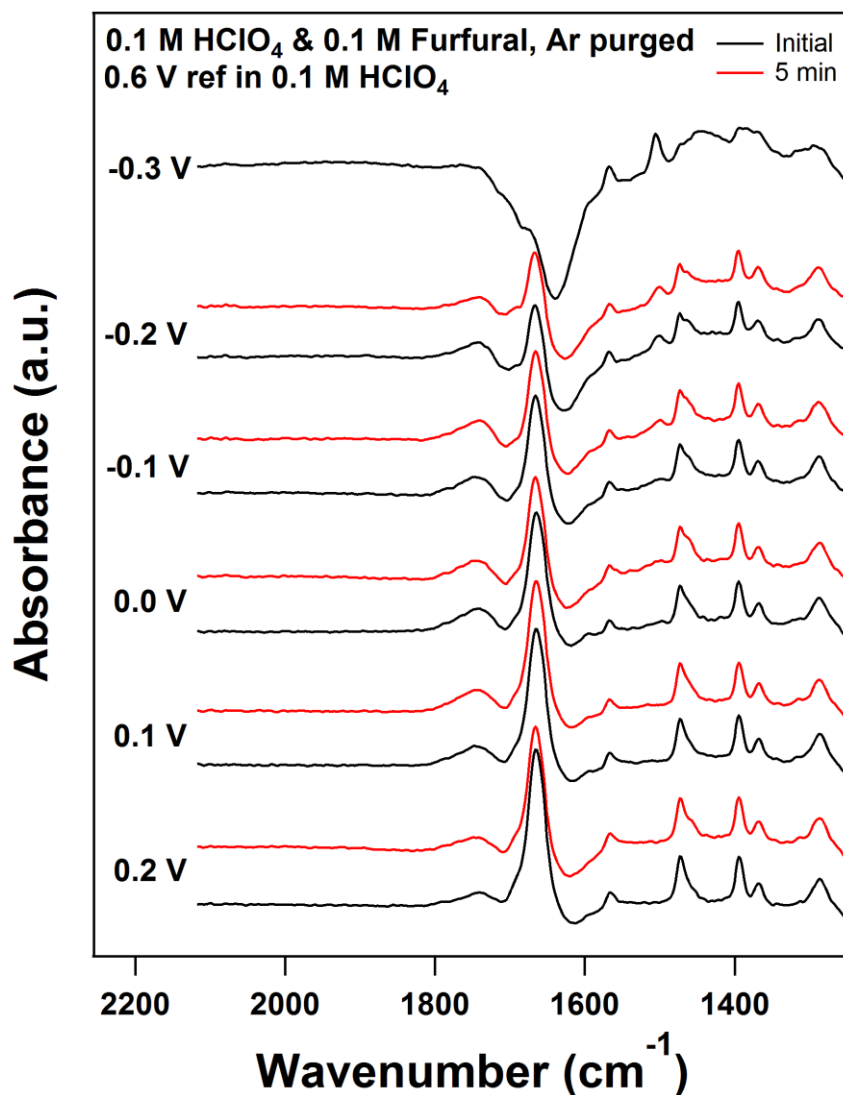


Figure 3.3 SEIRAS spectra of stepwise potential drop of 0.1 M HClO₄ and 0.1 M furfural solution on Au film, purged in Ar. Scans are initially taken (purple) and taken again after 5 minutes (red). Reference scan taken in 0.1 M HClO₄ at 0.6 V. Scans are taken at 4 cm⁻¹ wavenumber resolution.

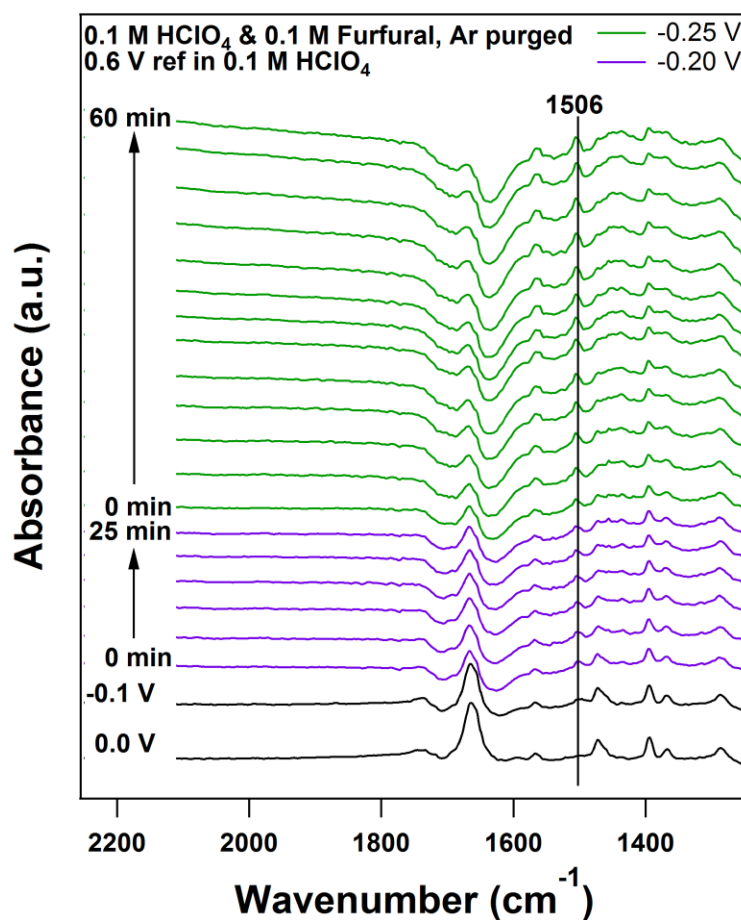


Figure 3.4 Time resolved SEIRAS spectra of furfural reduction on an Au film in a 0.1 M furfural and 0.1 M HClO₄ solution. Purple and green traces represent potentials of -0.2 and -0.25 respectively. Reference spectrum is taken at 0.6 V in 0.1 M HClO₄. 64 co-added scans, 4 cm⁻¹ resolution.

The 2-methylfuran stays near of the surface without adsorbing or dissipating with time. When 2-methylfuran is produced, changing the potential has little effect on the 1508 cm⁻¹ band related to 2-methylfuran (Figure 3.5). After the 2-methylfuran is first generated at -0.3 V, the potential is increased to 0.2 V, and increased by 0.2 V intervals until a potential of 1.2 V is reached. The 1508 cm⁻¹ band only starts to diminish 1.2 V. Changing the potential has no effect on wavenumber of the bands related to both

2-methylfuran and furfural, which would indicate that the species is adsorbed on the surface with a Stark Tuning effect⁷⁸.

3.4 Conclusion

The bands seen on Au are also similar to those seen in bulk versions of those species on a bare Si prism (Figure A.9). The strength of these bands and the overall low concentration indicates that there is high concentration band near the surface of Au that, for unknown reasons, cannot dissipate into the bulk of the electrolyte. This local high concentration could be indicative of the low production of 2-methylfuran on Au. This concentration density could prevent further furfural from reaching the surface, as the diminishing furfural bands show when 2-methylfuran bands increase. However, Au foil does continue to produce furfural as charge increases, but at a lower potential (Figure 3.1). Instead of the possible resinification that occurs at the higher potentials investigated spectroscopically, this low potential (-1.0 V) is most selective to hydrogen evolution. Increased hydrogen evolution may have some impact on this local concentration of 2-methylfuran near the electrode surface.

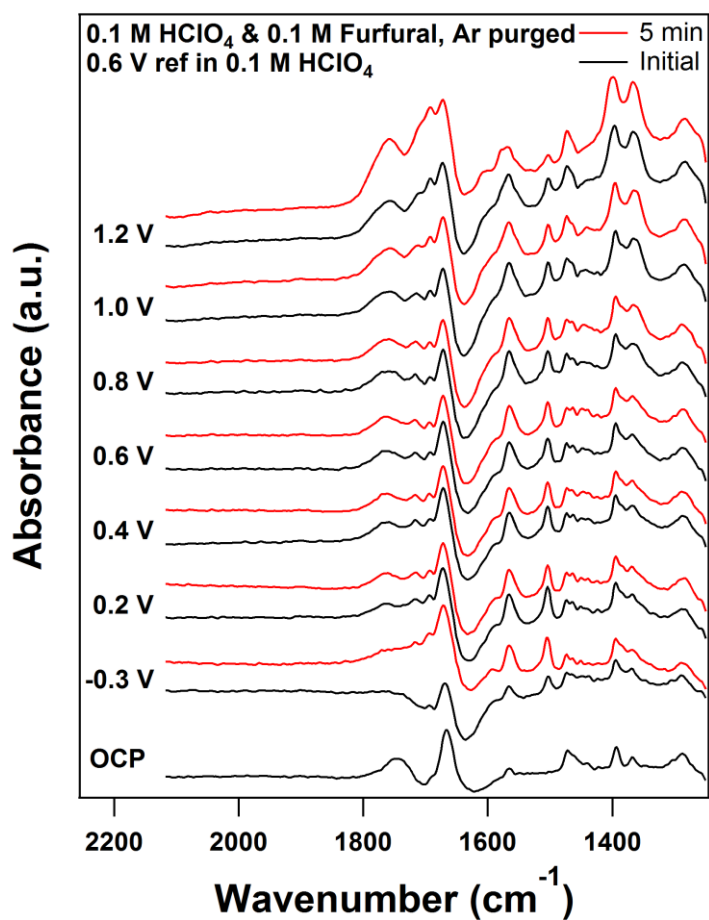


Figure 3.5 Time resolved SEIRAS scans of 2-methylfuran remaining near the Au surface as the potential is raised from initial production at -0.3 V. Black scans indicate the initial scan taken at the given potential; red traces indicate spectra taken after the potential is maintained for 5 minutes. Reference scan taken at 0.6 V in 0.1 M HClO₄. 64 co-added scans; 4 cm⁻¹ resolution.

Chapter 4

CONCLUDING REMARKS AND FURTHER RESEARCH

SEIRAS is a powerful technique for some aspects of green chemistry. On Cu, SEIRAS is able to identify a previously undocumented adsorbed hydrogen species that could affect the formation of the higher order fuel species produced in CO₂ reduction on that surface. In furfural reduction, SEIRAS is able to identify a local high concentration of 2-methylfuran while reducing furfural. This local high concentration could prohibit the overall reduction of furfural under these conditions. However, while investigating CO₂ reduction on Sn, SEIRAS was unable to detect anything that other *in-situ* techniques have been able to identify. SEIRAS is a powerful technique, but there are chemical systems where SEIRAS does not add insightful data.

Regardless, SEIRAS, and techniques of electrochemically depositing various metals on Au films, can be further tested. In the Sn system, only one deposition technique was investigated for the electrochemical deposition, and alternative systems which do not have the pinholes could promote further identification on the Sn surface. The Cu films are only viable at relatively low potentials (>-0.6 V), and alternative deposition techniques may allow for a more robust film to better analyze CO₂ reduction at potentials where more important products are made (<-0.9 V). Furthermore, more metals could be incorporated to investigate various primary product groups, such as Pd or Bi for further formate producing species or Zn or Pd for primarily CO/HCOO⁻ production⁹.

As for biomass conversion, only the initial studies for one reaction are presented in this work. Primary work could be conducted on a variety of systems, such as phenol reduction, HMF reduction, or HMF oxidation. Starting with systems that have

previously been shown to be functional for electrochemical functionality would be worthwhile, but once these systems are shown, more information could be derived from surface studies such as that presented in Chapter 3.

REFERENCES

1. Koga, O.; Matsuo, T.; Yamazaki, H.; Hori, Y. *Bull. Chem. Soc. Jpn.* **1998**, *71*, 315.
2. *Climate Change 2001: The Scientific Basis*. Cambridge University Press: Cambridge, United Kingdom, 2001.
3. Dr. Pieter Tans NOAA/ESRL and Dr. Ralph Keeling, Scripps Institution of Oceanography.
4. NOAA Earth System Research Laboratory.
5. *The Emissions Gap Report*; UNEP: 2015.
6. Finkenrath, M. *Cost and Performance of Carbon Dioxide Capture from Power Generation*; International Energy Agency: 2011.
7. Benson, S. M.; Cole, D. R. CO₂ Sequestration in Deep Sedimentary Formations. *Elements* **2008**, *4* (5), 325-331.
8. Whipple, D. T.; Kenis, P. J. A. Prospects of CO₂ utilization via direct heterogeneous electrochemical reduction. *J. Phys. Chem. Lett.* **2010**, *1* (24), 3451-3458.
9. Hori, Y. Electrochemical CO₂ reduction on metal electrodes. In *Modern aspects of electrochemistry*, Springer: 2008; pp 89-189.
10. Alonso, D. M.; Bond, J. Q.; Dumesic, J. A. Catalytic conversion of biomass to biofuels. *Green Chemistry* **2010**, *12* (9), 1493-1513.
11. Zaldivar, J.; Nielsen, J.; Olsson, L. Fuel ethanol production from lignocellulose: a challenge for metabolic engineering and process integration. *Applied Microbiology and Biotechnology* **2001**, *56* (1), 17-34.
12. van der Stelt, M. J. C.; Gerhauser, H.; Kiel, J. H. A.; Ptasiński, K. J. Biomass upgrading by torrefaction for the production of biofuels: A review. *Biomass and Bioenergy* **2011**, *35* (9), 3748-3762.
13. Oda, I.; Ogasawara, H.; Ito, M. Carbon monoxide adsorption on copper and silver electrodes during carbon dioxide electroreduction studied by infrared reflection absorption spectroscopy and surface-enhanced raman spectroscopy. *Langmuir* **1996**, *12* (4), 1094-1097.
14. Hori, Y.; Koga, O.; Aramata, A.; Enyo, M. Infrared spectroscopic observation of adsorbed CO intermediately formed in the electrochemical reduction of CO₂ at a nickel electrode. *Bull. Chem. Soc. Jpn.* **1992**, *65* (11), 3008-3010.
15. Davidson, T.; Pons, B. S.; Bewick, A.; Schmidt, P. P. Vibrational spectroscopy of the electrode/electrolyte interface. Use of fourier transform infrared spectroscopy. *J. Electroanal. Chem. Interfacial Electrochem.* **1981**, *125* (1), 237-241.
16. Hori, Y.; Koga, O.; Watanabe, Y.; Matsuo, T. FTIR measurements of charge displacement adsorption of CO on poly- and single crystal (100) of Cu electrodes. *Electrochim. Acta* **1998**, *44* (8-9), 1389-1395.
17. Hori, Y.; Koga, O.; Yamazaki, H.; Matsuo, T. Infrared spectroscopy of adsorbed CO and intermediate species in electrochemical reduction of CO₂ to hydrocarbons on a Cu electrode. *Electrochim. Acta* **1995**, *40* (16), 2617-2622.

18. Seki, H.; Kunitatsu, K.; Golden, W. G. A Thin-Layer Electrochemical Cell for Infrared Spectroscopic Measurements of the Electrode/Electrolyte Interface. *Applied Spectroscopy* **1985**, 39 (3), 437-443.
19. Osawa, M.; Ataka, K.-i.; Yoshii, K.; Yotsuyanagi, T. Surface-enhanced infrared ATR spectroscopy for in situ studies of electrode/electrolyte interfaces. *J. Electron. Spectrosc. Relat. Phenom.* **1993**, 64-65, 371-379.
20. Osawa, M. Dynamic processes in electrochemical reactions studied by surface-enhanced infrared absorption spectroscopy (SEIRAS). *Bull. Chem. Soc. Jpn.* **1997**, 70 (12), 2861-2880.
21. Osawa, M. Surface-enhanced infrared absorption. In *Near-Field Optics and Surface Plasmon Polaritons*, Kawata, S., Ed. Springer Berlin Heidelberg: Berlin, Heidelberg, 2001; pp 163-187.
22. Pons, S.; Davidson, T.; Bewick, A. Vibrational spectroscopy of the electrode-electrolyte interface. *J. Electroanal. Chem. Interfacial Electrochem.* **1984**, 160 (1), 63-71.
23. E. Kretschmann, H. R. Radiative decay of non radiative surface plasmons excited by light. *Z. Naturforsch* **1968**, 23 (12), 2135-2136.
24. Kretschmann, E. The angular dependence and the polarisation of light emitted by surface plasmons on metals due to roughness. *Optics Communications* **1972**, 5 (5), 331-336.
25. Bruns, R.; Raether, H. Plasma resonance radiation from non radiative plasmons. *Zeitschrift für Physik* **1970**, 237 (1), 98-106.
26. Ramanathan, V.; Coakley, J. A. Climate modeling through radiative-convective models. *Rev. Geophys.* **1978**, 16 (4), 465-489.
27. Jacobson, M. Z. Studying ocean acidification with conservative, stable numerical schemes for nonequilibrium air-ocean exchange and ocean equilibrium chemistry. *J. Geophys. Res. D* **2005**, 110 (D7), n/a-n/a.
28. Alsos, I. G.; Ehrich, D.; Thuiller, W.; Eidesen, P. B.; Tribsch, A.; Schönswetter, P.; Lagaye, C.; Taberlet, P.; Brochmann, C. Genetic consequences of climate change for northern plants. *Proc. R. Soc. B* **2012**.
29. Thomas, C. D.; Cameron, A.; Green, R. E.; Bakkenes, M.; Beaumont, L. J.; Collingham, Y. C.; Erasmus, B. F. N.; de Siqueira, M. F.; Grainger, A.; Hannah, L.; Hughes, L.; Huntley, B.; van Jaarsveld, A. S.; Midgley, G. F.; Miles, L.; Ortega-Huerta, M. A.; Townsend Peterson, A.; Phillips, O. L.; Williams, S. E. Extinction risk from climate change. *Nature* **2004**, 427 (6970), 145-148.
30. NOAA, Earth System Research Laboratory.
<http://www.esrl.noaa.gov/gmd/ccgg/trends/full.html> (accessed 03/11/16).
31. Vuuren, D. P.; Deetman, S.; Vliet, J.; Berg, M.; Ruijven, B. J.; Koelbl, B. The role of negative CO₂ emissions for reaching 2 °C—insights from integrated assessment modelling. *Clim. Chang.* **2013**, 118 (1), 15-27.
32. Hori, Y.; Murata, A.; Takahashi, R. Formation of hydrocarbons in the electrochemical reduction of carbon dioxide at a copper electrode in aqueous solution. *J. Chem. Soc., Faraday Trans.* **1989**, 85 (8), 2309-2326.

33. Hori, Y.; Murata, A.; Tsukamoto, T.; Wakebe, H.; Koga, O.; Yamazaki, H. Adsorption of carbon monoxide at a copper electrode accompanied by electron transfer observed by voltammetry and IR spectroscopy. *Electrochim. Acta* **1994**, *39* (17), 2495-2500.
34. Hori, Y.; Kikuchi, K.; Suzuki, S. Production of CO and CH₄ in electrochemical reduction of CO₂ at metal electrodes in aqueous hydrogencarbonate solution. *Chem. Lett.* **1985**, *14* (11), 1695-1698.
35. Kuhl, K. P.; Cave, E. R.; Abram, D. N.; Jaramillo, T. F. New insights into the electrochemical reduction of carbon dioxide on metallic copper surfaces. *Energ. Environ. Sci.* **2012**, *5* (5), 7050-7059.
36. Li, C. W.; Kanan, M. W. CO₂ reduction at low overpotential on Cu electrodes resulting from the reduction of thick Cu₂O films. *J. Am. Chem. Soc.* **2012**, *134* (17), 7231-7234.
37. Schouten, K. J. P.; Kwon, Y.; van der Ham, C. J. M.; Qin, Z.; Koper, M. T. M. A new mechanism for the selectivity to C1 and C2 species in the electrochemical reduction of carbon dioxide on copper electrodes. *Chem. Sci.* **2011**, *2* (10), 1902-1909.
38. Nie, X.; Esopi, M. R.; Janik, M. J.; Asthagiri, A. Selectivity of CO₂ reduction on copper electrodes: the role of the kinetics of elementary steps. *Angew. Chem. Int. Ed.* **2013**, *52* (9), 2459-2462.
39. Peterson, A. A.; Abild-Pedersen, F.; Studt, F.; Rossmeisl, J.; Nørskov, J. K. How copper catalyzes the electroreduction of carbon dioxide into hydrocarbon fuels. *Energy Environ. Sci.* **2010**, *3* (9), 1311-1315.
40. Azuma, M.; Hashimoto, K.; Hiramoto, M.; Watanabe, M.; Sakata, T. Electrochemical reduction of carbon dioxide on various metal electrodes in low-temperature aqueous KHCO₃ media. *J. Electrochem. Soc.* **1990**, *137* (6), 1772-1778.
41. Hori, Y.; Wakebe, H.; Tsukamoto, T.; Koga, O. Electrocatalytic process of CO selectivity in electrochemical reduction of CO₂ at metal electrodes in aqueous media. *Electrochim. Acta* **1994**, *39* (11), 1833-1839.
42. Jermann, B.; Augustynski, J. Long-term activation of the copper cathode in the course of CO₂ reduction. *Electrochim. Acta* **1994**, *39* (11), 1891-1896.
43. Kyriacou, G.; Anagnostopoulos, A. Electroreduction of CO₂ on differently prepared copper electrodes: The influence of electrode treatment on the current efficiencies. *J. Electroanal. Chem.* **1992**, *322* (1-2), 233-246.
44. Hori, Y.; Murata, A.; Yoshinami, Y. Adsorption of CO, intermediately formed in electrochemical reduction of CO₂, at a copper electrode. *J. Chem. Soc., Faraday Trans.* **1991**, *87* (1), 125-128.
45. Murata, A.; Hori, Y. Product selectivity affected by cationic species in electrochemical reduction of CO₂ and CO at a Cu electrode. *Bull. Chem. Soc. Jpn.* **1991**, *64* (1), 123-127.
46. Hori, Y.; Murata, A.; Takahashi, R.; Suzuki, S. Electroreduction of carbon monoxide to methane and ethylene at a copper electrode in aqueous solutions at ambient temperature and pressure. *J. Am. Chem. Soc.* **1987**, *109* (16), 5022-5023.

47. Watanabe, K.; Nagashima, U.; Hosoya, H. An ab initio study of interactions of carbon monoxide and metal electrodes. *Chem. Phys. Lett.* **1993**, *209* (1–2), 109–110.
48. Watanabe, K.; Nagashima, U.; Hosoya, H. An ab initio study of adsorbed carbon monoxide on a metal electrode by cluster model. *Appl. Surf. Sci.* **1994**, *75* (1), 121–124.
49. Kim, J. J.; Summers, D. P.; Frese Jr, K. W. Reduction of CO₂ and CO to methane on Cu foil electrodes. *J. Electroanal. Chem. Interfacial Electrochem.* **1988**, *245* (1–2), 223–244.
50. DeWulf, D. W.; Jin, T.; Bard, A. J. Electrochemical and surface studies of carbon dioxide reduction to methane and ethylene at copper electrodes in aqueous solutions. *J. Electrochem. Soc.* **1989**, *136* (6), 1686–1691.
51. Cook, R. L.; MacDuff, R. C.; Sammells, A. F. On the electrochemical reduction of carbon dioxide at in situ electrodeposited copper. *J. Electrochem. Soc.* **1988**, *135* (6), 1320–1326.
52. Hori, Y.; Takahashi, R.; Yoshinami, Y.; Murata, A. Electrochemical reduction of CO at a copper electrode. *J. Phys. Chem. B* **1997**, *101* (36), 7075–7081.
53. Tang, W.; Peterson, A. A.; Varela, A. S.; Jovanov, Z. P.; Bech, L.; Durand, W. J.; Dahl, S.; Nørskov, J. K.; Chorkendorff, I. The importance of surface morphology in controlling the selectivity of polycrystalline copper for CO₂ electroreduction. *Phys. Chem. Chem. Phys.* **2012**, *14* (1), 76–81.
54. Li, C. W.; Ciston, J.; Kanan, M. W. Electroreduction of carbon monoxide to liquid fuel on oxide-derived nanocrystalline copper. *Nature* **2014**, *508* (7497), 504–507.
55. Hammer, B.; Morikawa, Y.; Nørskov, J. K. CO chemisorption at metal surfaces and overlayers. *Phys. Rev. Lett.* **1996**, *76* (12), 2141–2144.
56. Hori, Y.; Wakebe, H.; Tsukamoto, T.; Koga, O. Adsorption of CO accompanied with simultaneous charge transfer on copper single crystal electrodes related with electrochemical reduction of CO₂ to hydrocarbons. *Surf. Sci.* **1995**, *335*, 258–263.
57. Salimon, J.; Kalaji, M. Electrochemical behavior of polycrystalline copper in aqueous phosphate buffered solution during CO₂ reduction. *Pertanika J. Sci. Technol.* **2003**, *11* (1), 135–144.
58. Hernandez R, R. M.; Kalaji, M. Use of isotopically labelled compounds for the in situ IR study of the electroreduction of CO₂ in aqueous hydrogencarbonate and buffered phosphate solutions. *J. Chem. Soc., Faraday Trans.* **1996**, *92* (20), 3957–3962.
59. Tory, J.; Setterfield-Price, B.; Dryfe, R. A. W.; Hartl, F. [M(CO)₄(2,2'-bipyridine)] (M=Cr, Mo, W) complexes as efficient catalysts for electrochemical reduction of CO₂ at a gold electrode. *ChemElectroChem* **2015**, *2* (2), 213–217.
60. Vollmer, M. V.; Machan, C. W.; Clark, M. L.; Antholine, W. E.; Agarwal, J.; Iii, H. F. S.; Kubiak, C. P.; Walensky, J. R. Synthesis, spectroscopy, and electrochemistry of (α-Diimine)M(CO)₃Br, M = Mn, Re, complexes: ligands isoelectronic to bipyridyl show differences in CO₂ reduction. *Organometallics* **2015**, *34* (1), 3–12.
61. Ampelli, C.; Genovese, C.; Errahali, M.; Gatti, G.; Marchese, L.; Perathoner, S.; Centi, G. CO₂ capture and reduction to liquid fuels in a novel electrochemical setup

- by using metal-doped conjugated microporous polymers. *J. Appl. Electrochem.* **2015**, 45 (7), 701-713.
62. Nikolic, B. Z.; Huang, H.; Gervasio, D.; Lin, A.; Fierro, C.; Adzic, R. R.; Yeager, E. Electroreduction of carbon dioxide on platinum single crystal electrodes: electrochemical and in situ FTIR studies. *J. Electroanal. Chem. Interfacial Electrochem.* **1990**, 295 (1), 415-423.
 63. Ortiz, R.; Márquez, O. P.; Márquez, J.; Gutiérrez, C. FTIR spectroscopy study of the electrochemical reduction of CO₂ on various metal electrodes in methanol. *J. Electroanal. Chem.* **1995**, 390 (1-2), 99-107.
 64. Baruch, M. F.; Pander, J. E.; White, J. L.; Bocarsly, A. B. Mechanistic insights into the reduction of CO₂ on tin electrodes using in situ ATR-IR spectroscopy. *ACS Catal.* **2015**, 5 (5), 3148-3156.
 65. Rosen, B. A.; Haan, J. L.; Mukherjee, P.; Braunschweig, B.; Zhu, W.; Salehi-Khojin, A.; Dlott, D. D.; Masel, R. I. In situ spectroscopic examination of a low overpotential pathway for carbon dioxide conversion to carbon monoxide. *J. Phys. Chem. C* **2012**, 116 (29), 15307-15312.
 66. Rosen, B. A.; Salehi-Khojin, A.; Thorson, M. R.; Zhu, W.; Whipple, D. T.; Kenis, P. J. A.; Masel, R. I. Ionic Liquid-Mediated Selective Conversion of CO₂ to CO at Low Overpotentials. *Science* **2011**, 334 (6056), 643-644.
 67. Figueiredo, M. C.; Ledezma-Yanez, I.; Koper, M. T. M. In situ spectroscopic study of CO₂ electroreduction at copper electrodes in acetonitrile. *ACS Catal.* **2016**.
 68. Miyake, H.; Osawa, M. Surface-enhanced infrared spectrum of CO adsorbed on Cu electrodes in solution. *Chem. Lett.* **2004**, 33 (3), 278-279.
 69. Wang, H.-F.; Yan, Y.-G.; Huo, S.-J.; Cai, W.-B.; Xu, Q.-J.; Osawa, M. Seeded growth fabrication of Cu-on-Si electrodes for in situ ATR-SEIRAS applications. *Electrochim. Acta* **2007**, 52 (19), 5950-5957.
 70. Smolinka, T.; Heinen, M.; Chen, Y. X.; Jusys, Z.; Lehnert, W.; Behm, R. J. CO₂ reduction on Pt electrocatalysts and its impact on H₂ oxidation in CO₂ containing fuel cell feed gas – A combined in situ infrared spectroscopy, mass spectrometry and fuel cell performance study. *Electrochim. Acta* **2005**, 50 (25-26), 5189-5199.
 71. Miyake, H.; Ye, S.; Osawa, M. Electroless deposition of gold thin films on silicon for surface-enhanced infrared spectroelectrochemistry. *Electrochem. Commun.* **2002**, 4 (12), 973-977.
 72. Dunwell, M.; Yan, Y.; Xu, B. A surface-enhanced infrared absorption spectroscopic study of pH dependent water adsorption on Au. *Surf. Sci.*
 73. Nagahara, L. A.; Ohmori, T.; Hashimoto, K.; Fujishima, A. Effects of HF solution in the electroless deposition process on silicon surfaces. *J. Vac. Sci. Technol. A* **1993**, 11 (4), 763-767.
 74. Yan; Li, Q.-X.; Huo, S.-J.; Ma, M.; Cai, W.-B.; Osawa, M. Ubiquitous strategy for probing ATR surface-enhanced infrared absorption at platinum group metal-electrolyte interfaces. *J. Phys. Chem. B* **2005**, 109 (16), 7900-7906.
 75. Sun, S.-G.; Cai, W.-B.; Wan, L.-J.; Osawa, M. Infrared absorption enhancement for CO adsorbed on Au films in perchloric acid solutions and effects of surface structure

- studied by cyclic voltammetry, scanning tunneling microscopy, and surface-enhanced IR spectroscopy. *J. Phys. Chem. B* **1999**, *103* (13), 2460-2466.
76. Mills, J. N.; McCrum, I. T.; Janik, M. J. Alkali cation specific adsorption onto fcc(111) transition metal electrodes. *Phys. Chem. Chem. Phys.* **2014**, *16* (27), 13699-13707.
 77. Akhade, S. A.; McCrum, I. T.; Janik, M. J. The impact of specifically adsorbed ions on the copper-catalyzed electroreduction of CO₂. *J. Electrochem. Soc.* **2016**, *163* (6), F477-F484.
 78. Lambert, D. K. Vibrational Stark effect of adsorbates at electrochemical interfaces. *Electrochim. Acta* **1996**, *41* (5), 623-630.
 79. Arihara, K.; Kitamura, F.; Ohsaka, T.; Tokuda, K. Characterization of the adsorption state of carbonate ions at the Au(111) electrode surface using in situ IRAS. *J. Electroanal. Chem.* **2001**, *510* (1-2), 128-135.
 80. Grabow, L. C.; Mavrikakis, M. Mechanism of Methanol Synthesis on Cu through CO₂ and CO Hydrogenation. *ACS Catalysis* **2011**, *1* (4), 365-384.
 81. Dixon, L. T.; Barth, R.; Gryder, J. W. Infrared active species of hydrogen adsorbed by alumina-supported platinum. *Journal of Catalysis* **1975**, *37* (2), 368-375.
 82. McCrum, I. T.; Janik, M. J. pH and alkali cation effects on the Pt cyclic voltammogram explained using density functional theory. *J. Phys. Chem. C* **2016**, *120* (1), 457-471.
 83. Strmcnik D; Kodama K; van der Vliet, D.; Greeley J; Stamenkovic, V. R.; Marković, N. M. The role of non-covalent interactions in electrocatalytic fuel-cell reactions on platinum. *Nat. Chem.* **2009**, *1* (6), 466-472.
 84. Thorson, M. R.; Siil, K. I.; Kenis, P. J. A. Effect of cations on the electrochemical conversion of CO₂ to CO. *J. Am. Chem. Soc.* **2013**, *160* (1), F69-F74.
 85. Sandl, P.; Bischler, U.; Bertel, E. The interaction of atomic hydrogen with Cu(110). *Surf. Sci.* **1993**, *291* (1), 29-38.
 86. Tin Prices and Tin Price Charts. <http://www.infomine.com/investment/metal-prices/tin/> (accessed 10-19).
 87. He, A.; Liu, Q.; Ivey, D. G. Electrodeposition of tin: a simple approach. *Journal of Materials Science: Materials in Electronics* **2008**, *19* (6), 553-562.
 88. Marek, G.; Andreas, E.; Jürgen, H. CO adsorption on close-packed transition and noble metal surfaces: trends from ab initio calculations. *J. Phys. Condens. Matter* **2004**, *16* (8), 1141.
 89. Climent, M. J.; Corma, A.; Iborra, S. Conversion of biomass platform molecules into fuel additives and liquid hydrocarbon fuels. *Green Chemistry* **2014**, *16* (2), 516-547.
 90. Gruter, G. EP Pat, 1834950, 2007; GJM Gruter and F. Dautzenberg. *EP Pat* **2007**, *1834951*.
 91. Albert, W. C.; Lowy, A. The Electrochemical Reduction of Furfural. *Transactions of The Electrochemical Society* **1939**, *75* (1), 367-375.
 92. Chamoulaud, G.; Floner, D.; Moinet, C.; Lamy, C.; Belgsir, E. M. Biomass conversion II: simultaneous electrosyntheses of furoic acid and furfuryl alcohol on modified graphite felt electrodes. *Electrochimica Acta* **2001**, *46* (18), 2757-2760.

93. Parpot, P.; Bettencourt, A. P.; Chamoulaud, G.; Kokoh, K. B.; Belgsir, E. M. Electrochemical investigations of the oxidation–reduction of furfural in aqueous medium: Application to electrosynthesis. *Electrochimica Acta* **2004**, *49* (3), 397-403.
94. zhao, B.; Chen, M.; Guo, Q.; Fu, Y. Electrocatalytic hydrogenation of furfural to furfuryl alcohol using platinum supported on activated carbon fibers. *Electrochimica Acta* **2014**, *135*, 139-146.
95. Green, S. K.; Lee, J.; Kim, H. J.; Tompsett, G. A.; Kim, W. B.; Huber, G. W. The electrocatalytic hydrogenation of furanic compounds in a continuous electrocatalytic membrane reactor. *Green Chemistry* **2013**, *15* (7), 1869-1879.
96. Li, Z.; Kelkar, S.; Lam, C. H.; Luczek, K.; Jackson, J. E.; Miller, D. J.; Saffron, C. M. Aqueous electrocatalytic hydrogenation of furfural using a sacrificial anode. *Electrochimica Acta* **2012**, *64*, 87-93.
97. Scaranto, J.; Mavrikakis, M. Density functional theory studies of HCOOH decomposition on Pd(111). *Surface Science* **2016**, *650*, 111-120.
98. Kwon, Y.; Birdja, Y. Y.; Raoufmoghaddam, S.; Koper, M. T. M. Electrocatalytic Hydrogenation of 5-Hydroxymethylfurfural in Acidic Solution. *ChemSusChem* **2015**, *8* (10), 1745-1751.

Appendix A

SUPPORTING INFORMATION

This appendix serves as supporting information for this thesis. The first 8 figures are adapted with permission from Heyes, J.; Dunwell, M.; Xu, B. CO₂ Reduction on Cu at Low Overpotentials with Surface-Enhanced in Situ Spectroscopy. *The Journal of Physical Chemistry C* **2016**, *120* (31), 17334-17341.). Copyright 2016 American Chemical Society. The figures following that have not been previously published.

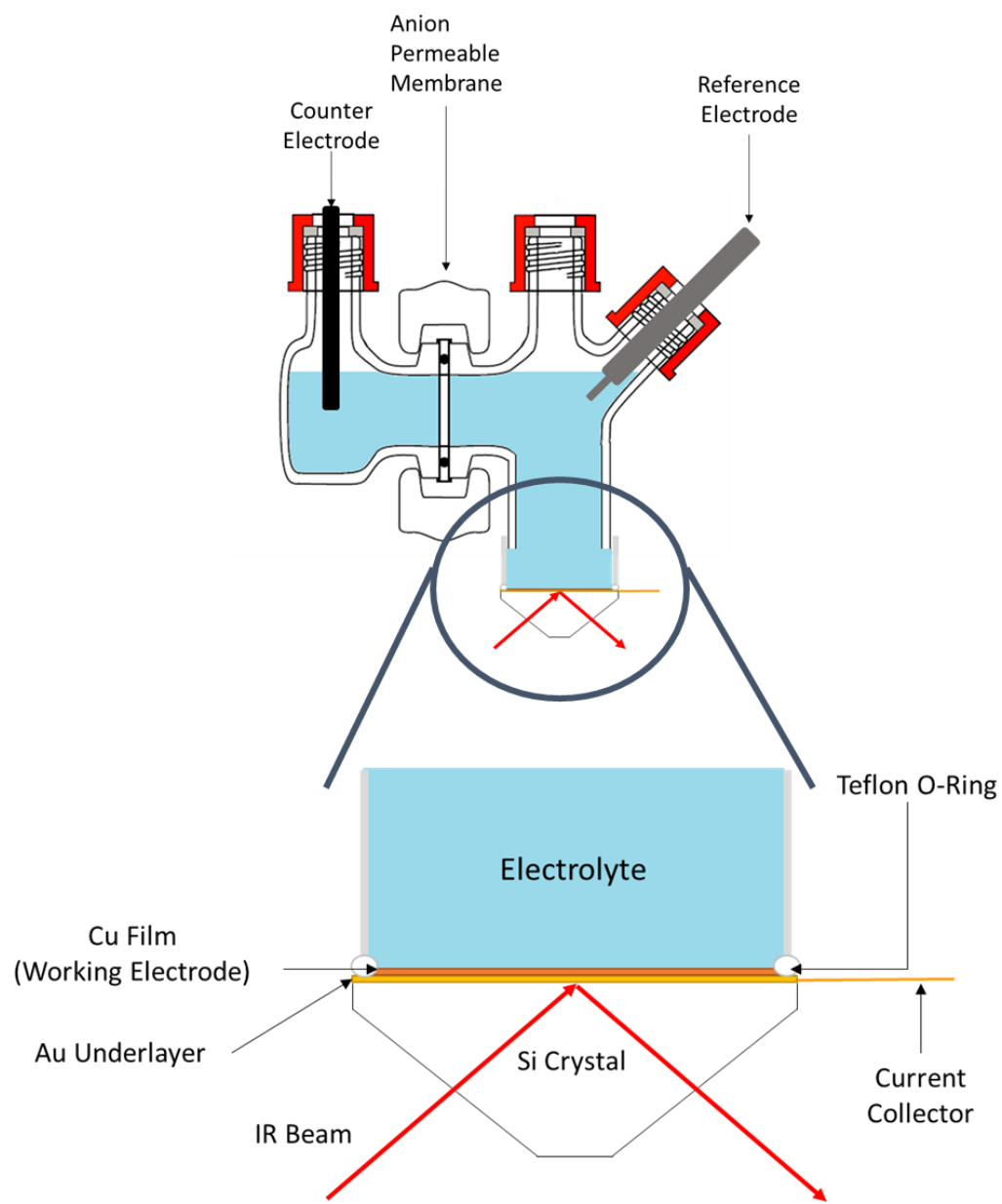


Figure A.1 Schematic of the experimental setup used for SEIRAS experiments

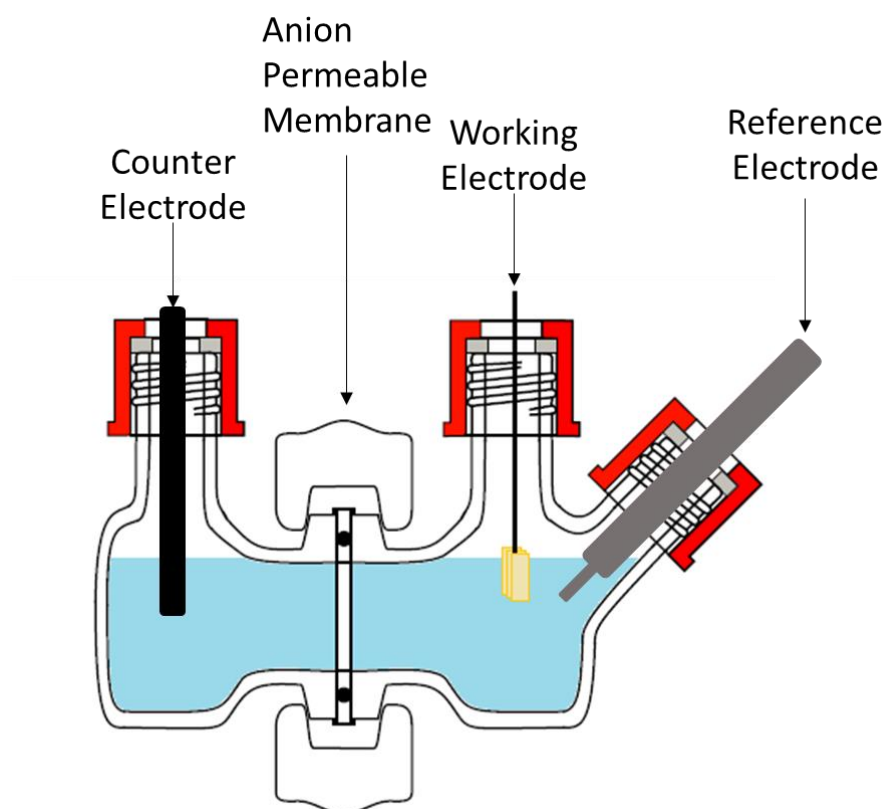


Figure A.2 Schematic of the H-cell used for selectivity studies. Not pictured are two additional ports for headspace sampling and purging on the same side of the membrane as the working electrode.

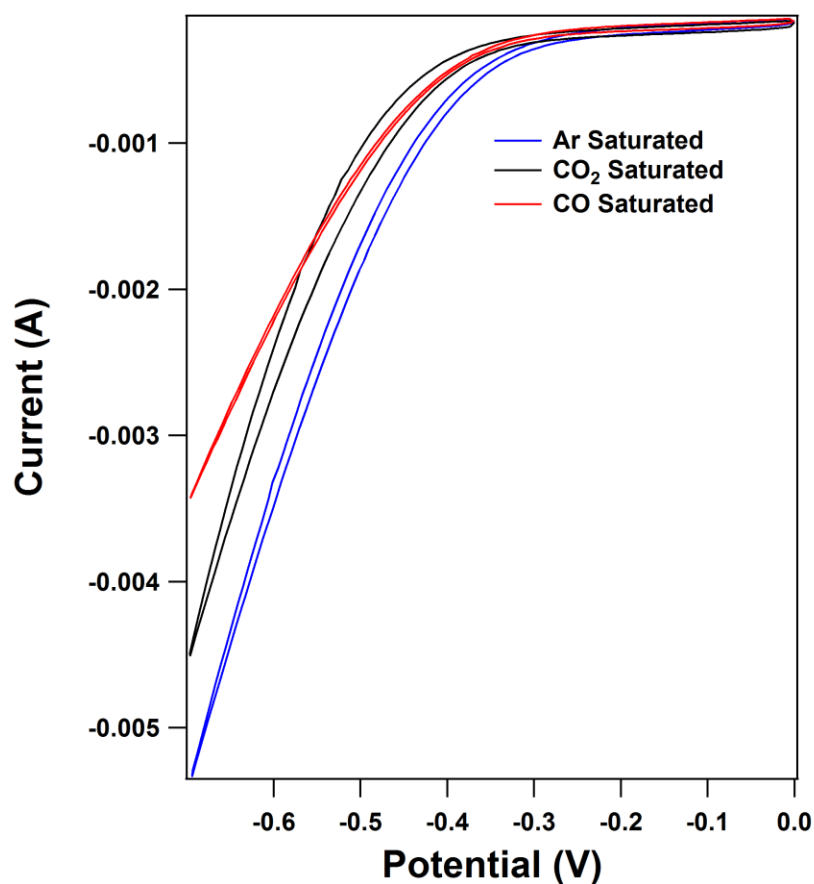


Figure A.3 Cyclic voltammogram of 0.5 M NaHCO₃ on electrochemically deposited Cu film saturated in Ar, CO₂ and CO. The retardation of HER activity in the CO₂ saturated electrolyte could be a CO₂ reductive intermediate effect. CO similarly retards these reactions by site blocking for HER with a CO_{ad} species.

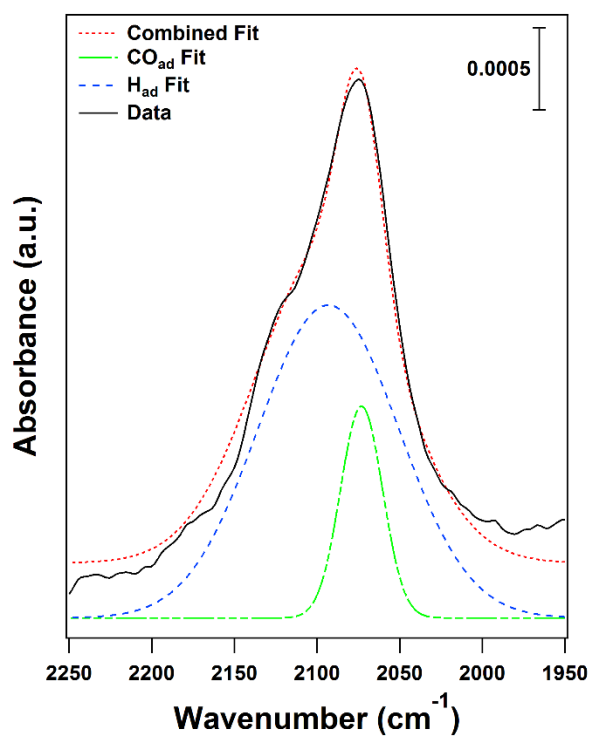


Figure A.4 Peak deconvolution of Figure 2.1.5a(vii). Similar procedure was conducted for the rest of spectra in Figure 2.1.6a. Figure 2.1.6c are calculated based on the quantification of these deconvoluted peaks. Peak widths of the H_{ad} and CO_{ad} are fixed in the fitting, and similar procedure was employed in the fitting of Figure A.5.

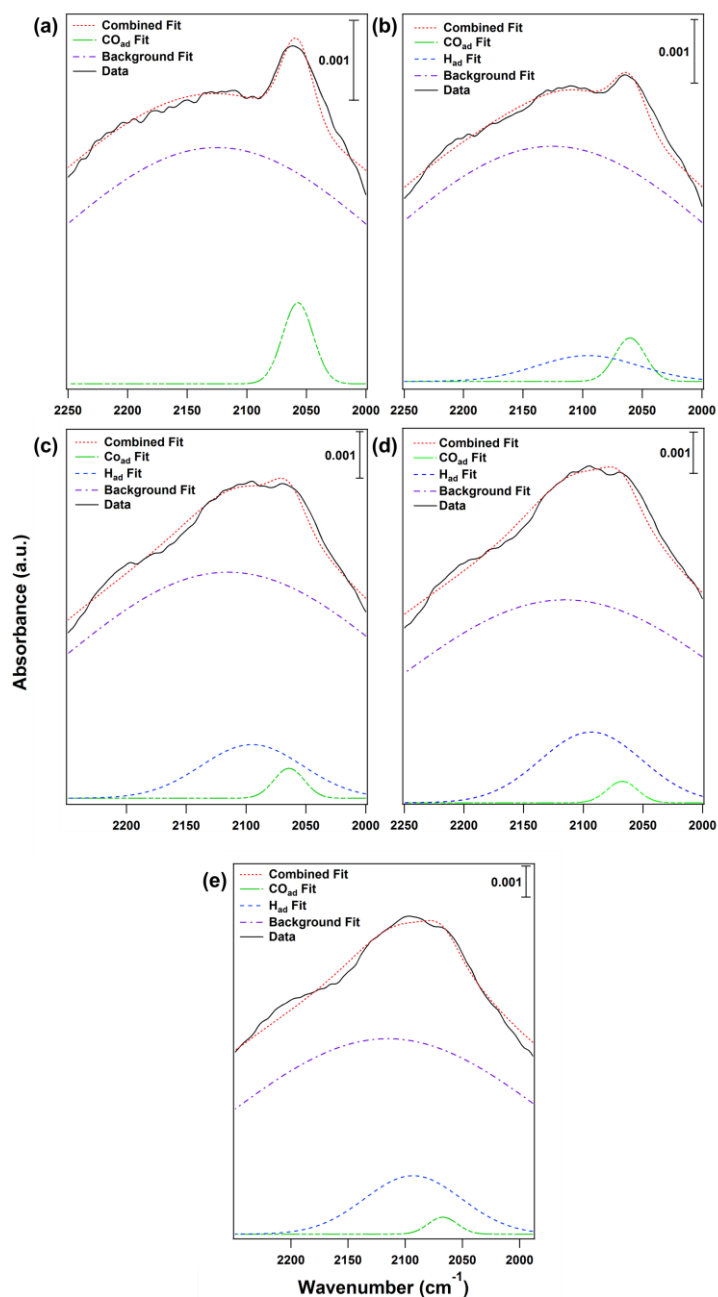


Figure A.5 Fitting of spectra in Figure 2.5b at times: 0 min (a), 5 min (b), 15 min (c), 25 min (d). Background fit is attributed to broad water character seen in Figure A.6. Note that the broad envelope from 2200-1975 cm^{-1} in Figure 2.6 is due to water rather than the H_{ad} or CO_{ad} band, which is confirmed by the spectrum of pure water. This broad band was removed in the peak deconvolution and quantification.

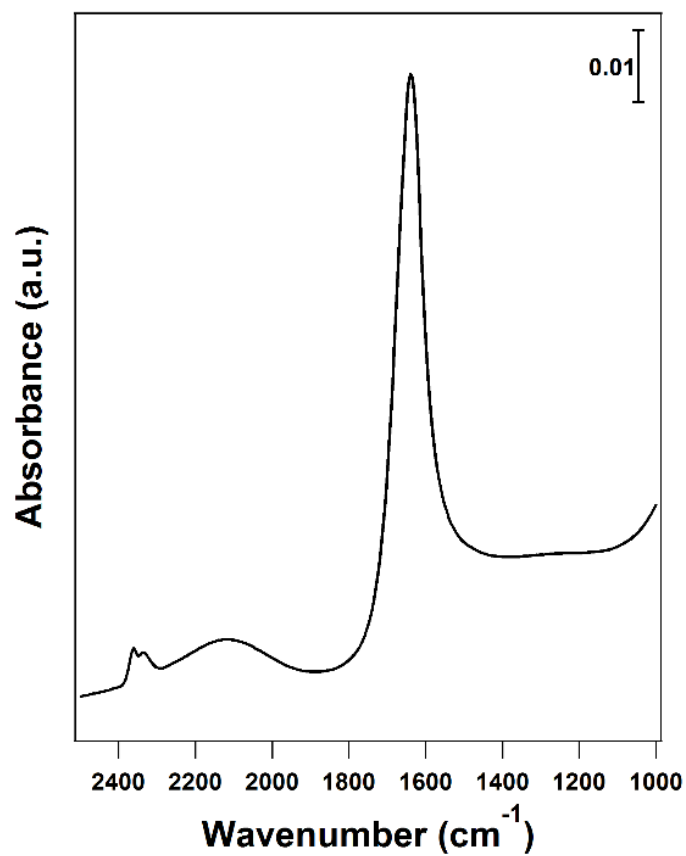


Figure A.6 Single reflectance ATR-FTIR spectra of H₂O on ZnSe prism, 4 cm⁻¹ resolution. Peak centered at approx. 2350 cm⁻¹ is ambient CO₂ present in apparatus

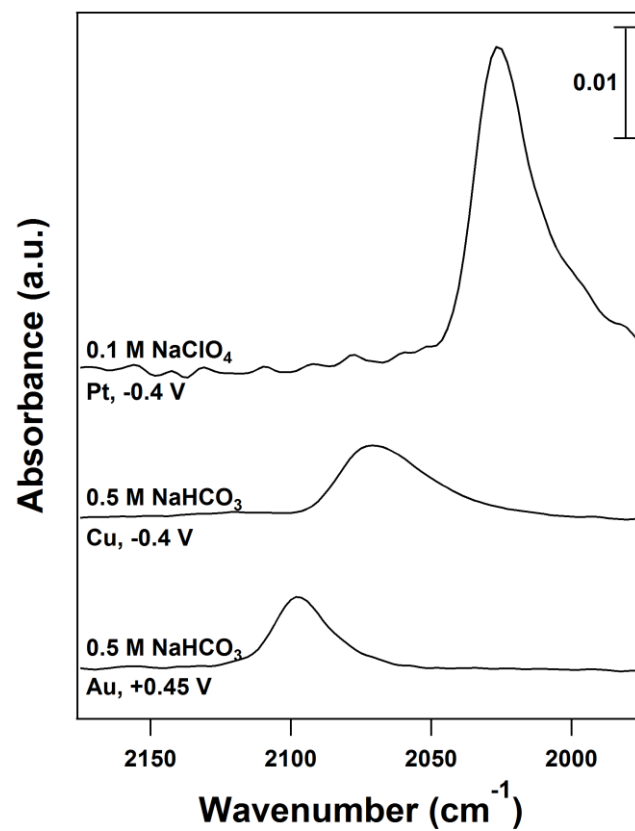


Figure A.7 SEIRAS spectral comparison of CO_{ad} on Pt, Cu, and Au surfaces at indicated potentials.

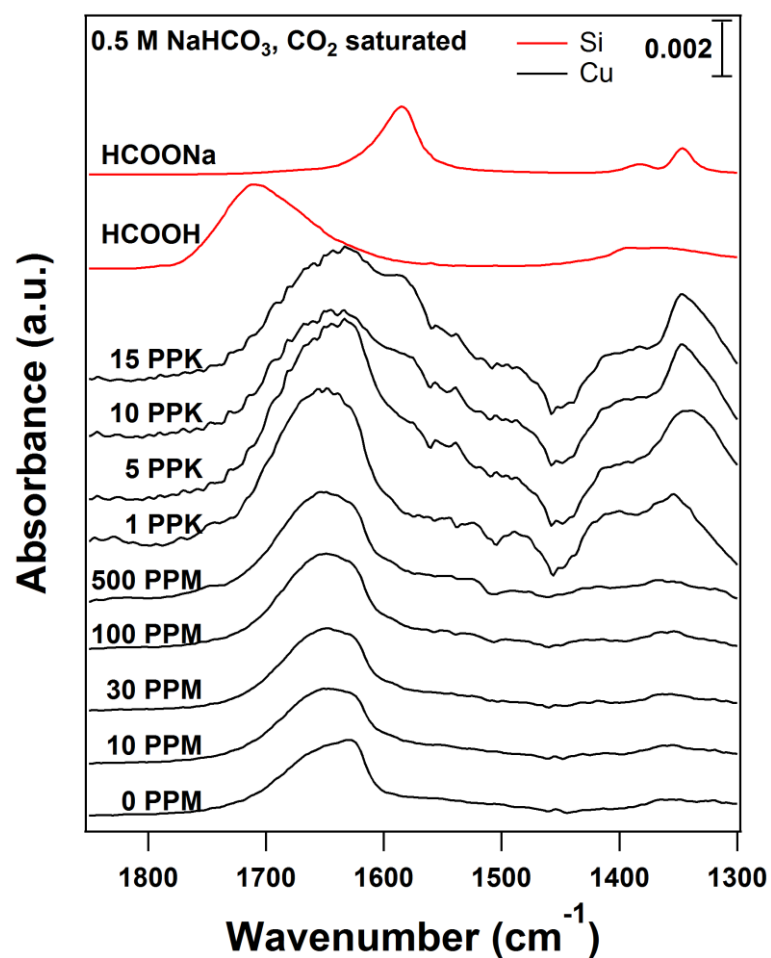


Figure A.8 SEIRAS spectra (black traces) of 0.5 M NaHCO₃ on Cu film with varying amounts of introduced formic acid at -0.4 V, with reference taken at -0.1 V in 0.5 M NaHCO₃ prior to the introduction of formic acid. Concentrations are indicated by volume. ATR spectra of 0.1 M HCOONa and HCOOH on a Si crystal (red traces) are included for comparison.

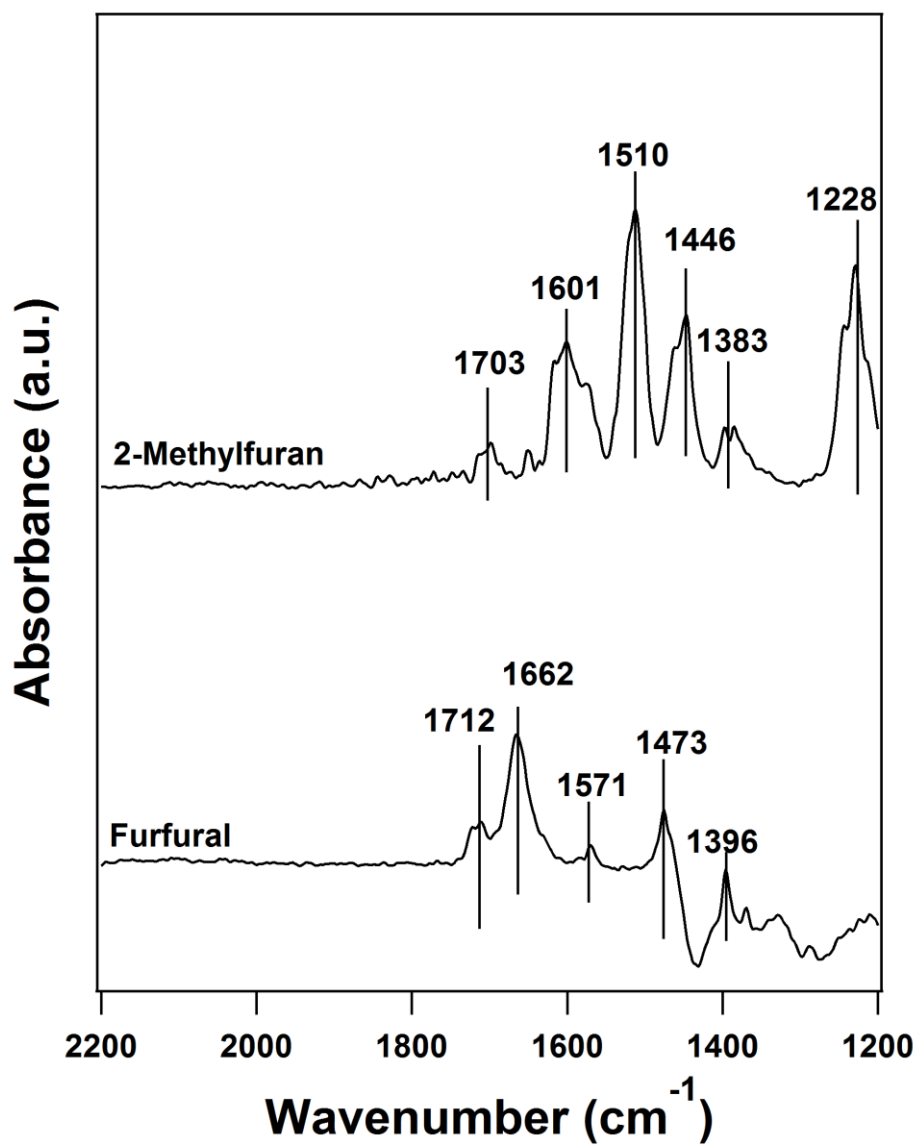


Figure A.9 FTIR spectra of furfural and 2-methylfuran diluted with 0.1 M HClO₄ on Si prism. 0.1 M HClO₄ background, 64 co-added scans, 4 cm⁻¹ wavenumber resolution.

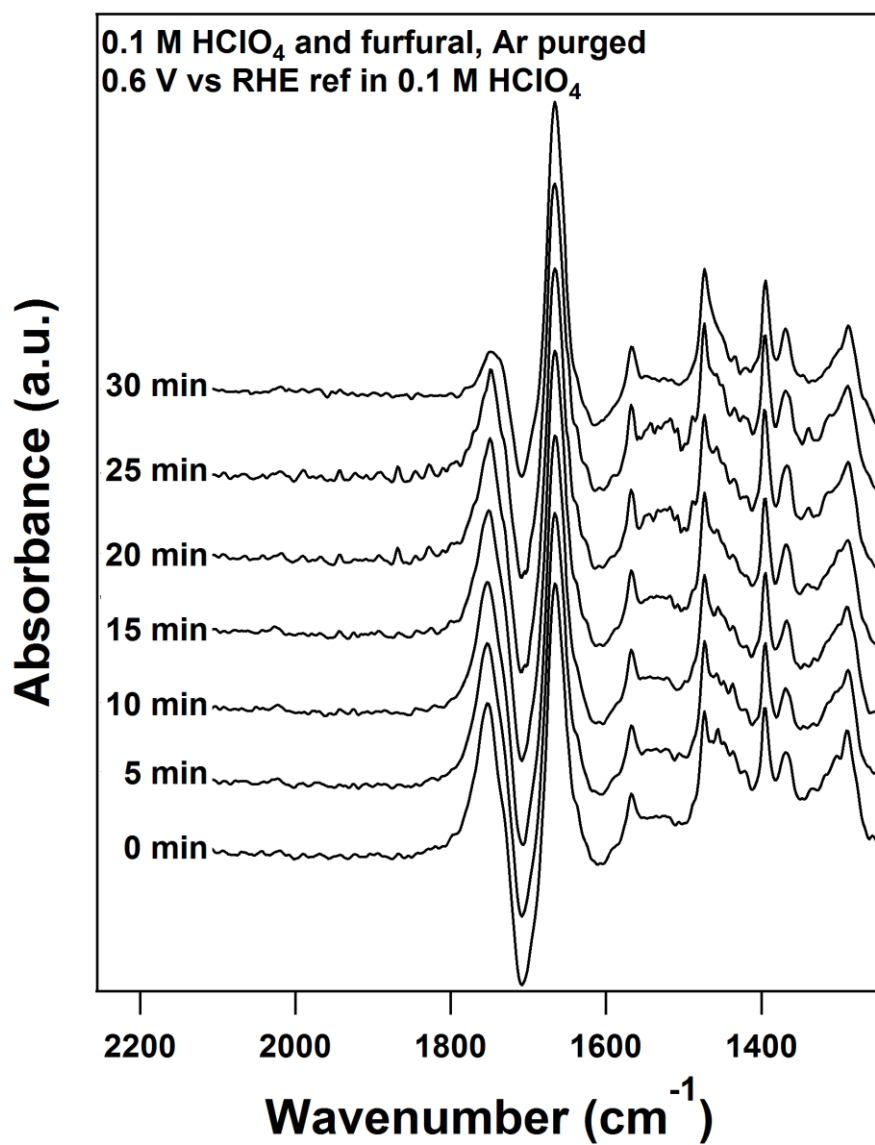




Figure A.10 Time resolved SEIRAS spectra of 0.1 M furfural in 0.1 M HClO₄ at open circuit potential. Reference taken at 0.6 V in 0.1 M HClO₄. 64 co-added scans, 4 cm⁻¹ wavenumber resolution


Appendix B


LEGAL PERMISSION

Rightslink® by Copyright Clearance Center

<https://s100.copyright.com>



[Home](#) [Create Account](#) [Help](#) 



Title: CO2 Reduction on Cu at Low Overpotentials with Surface-Enhanced in Situ Spectroscopy

Author: Jeffrey Heyes, Marco Dunwell, Bingjun Xu

Publication: The Journal of Physical Chemistry C

Publisher: American Chemical Society

Date: Aug 1, 2016

Copyright © 2016, American Chemical Society

LOGIN

If you're a [copyright.com](#) user, you can login to RightsLink using your [copyright.com](#) credentials. Already a [RightsLink](#) user or want to [learn more?](#)

PERMISSION/LICENSE IS GRANTED FOR YOUR ORDER AT NO CHARGE

This type of permission/license, instead of the standard Terms & Conditions, is sent to you because no fee is being charged for your order. Please note the following:

- Permission is granted for your request in both print and electronic formats, and translations.
- If figures and/or tables were requested, they may be adapted or used in part.
- Please print this page for your records and send a copy of it to your publisher/graduate school.
- Appropriate credit for the requested material should be given as follows: "Reprinted (adapted) with permission from (COMPLETE REFERENCE CITATION). Copyright (YEAR) American Chemical Society." Insert appropriate information in place of the capitalized words.
- One-time permission is granted only for the use specified in your request. No additional uses are granted (such as derivative works or other editions). For any other uses, please submit a new request.

[BACK](#)

[CLOSE WINDOW](#)

Copyright © 2016 [Copyright Clearance Center, Inc.](#) All Rights Reserved. [Privacy statement](#). [Terms and Conditions](#).
Comments? We would like to hear from you. E-mail us at customercare@copyright.com